Immunodetection in paper-based devices using Carbohydrate Binding Modules fusions for antibody anchoring and gold nanoparticles for colorimetric reporting

António Ricardo Marques Almeida

Thesis to obtain the Master of Science Degree in

Biotechnology

Supervisors: Prof. Duarte Miguel de França Teixeira dos Prazeres

Dra. Ana Margarida Nunes da Mata Pires de Azevedo

Examination Comittee

Chairperson: Prof. Leonilde de Fátima Morais Moreira

Supervisor: Prof. Duarte Miguel de França Teixeira dos Prazeres

Member of the Committee: Prof. Gabriel António Amaro Monteiro

December 2015

Aknowledgements

I would like to thank my supervisors Prof. Miguel Prazeres and Prof. Ana Azevedo for accepting me in this project, for the guidance and patience.

I would also like to thank my lab colleagues for providing a friendly and cooperative atmosphere, and especially to Ana Rosa for all the useful feedback and insightful comments on my work.

Finally, I want to thank my family and friends for all the support given throughout my academic life.

Abstract

There is a global demand for affordable, sensitive, selective and rapid analytical platforms usable in low-tech contexts to perform health diagnostics, environmental monitoring and food quality testing. Paper-based analytical devices (PADs) have emerged as one of such platforms, with the additional advantages of being biodegradable, easy-to-use and portable. Paper can be modified and adapted to perform biological assays by adding appropriate biorecognition and reporting agents to the test areas, but an underlying problem is the orientation of the biomolecules in the paper matrix. This can be solved by fusing the biorecognition element with protein domains like carbohydrate-binding modules (CBMs), which have high affinity for cellulose. One example is CBM3-ZZ, a fusion protein that combines the cellulose-binding properties of CBM3a from *C. thermocellum* with the antibody-binding properties of a double Z-domain from the staphylococcal protein A.

Wax printing was used to delineate circular reaction areas (spots) and microchannels on paper. Then anti-biotin antibodies were anchored on paper via the CBM3-ZZ fusion and its ability to recognize biotin was tested using gold nanoparticles coated with biotin (biotin-AuNPs). The capture of biotin-AuNPs by the CBM3-ZZ:antibiotin IgG complex in both the spot and microchannel configuration could be visually detected by the generation of a red color that is virtually absent in controls. These results open up the possibility of combining CBMs and gold nanoparticles with PADs for immunodetection purposes.

Keywords: Immunoassays, Paper-based analytical devices, Carbohydrate-binding modules, ZZ-domains, Gold nanoparticles.

Resumo

Existe uma demanda global de plataformas analíticas acessíveis, sensíveis, selectivas e rápidas para diagnóstico de saúde, analíse ambiental ou testes de qualidade dos alimentos. Os dispositivos analíticos baseados em papel (PADs) surgiram como uma destas plataformas, com as vantagens adicionais de serem biodegradáveis, fáceis de usar e portáteis. O papel pode ser modificado e adaptado para realizar ensaios biológicos adicionando um elemento de reconhecimento biomolecular adequado e um agente reporter para as áreas de teste, mas um problema subjacente é a orientação das biomoléculas na matriz de papel. Isto pode ser resolvido através da fusão dos elementos de reconhecimento biomolecular com domínios de proteínas como por exemplo, módulos de ligação a carbohidratos (CBMs), que têm uma elevada afinidade para a celulose. Um exemplo é CBM3-ZZ, uma proteína que combina as propriedades de ligação à celulose de CBM3a de *C. thermocellum*, com as propriedades de ligação de anticorpos de um duplo domínio-Z da proteína A.

Impressão de cera foi utilizado para delinear áreas circulares de reacção (spots) e microcanais em papel. Em seguida, anticorpos antibiotina foram imobilizados no papel através da fusão CBM3-ZZ e a sua capacidade para reconhecer a biotina foi testada utilizando nanopartículas de ouro revestidas com biotina (biotina-AuNPs). A captura de biotina-AuNPs pelo complexo CBM3-ZZ: antibiotina tanto em spots como em microcanais pode ser detectada visualmente através da geração de uma cor vermelha que é praticamente ausente nos controlos. Estes resultados abrem a possibilidade de combinar CBMs e nanopartículas de ouro com PADs para fins de imunodetecção.

Palavras-chave: Imunoensaios, Dispositivos analíticos baseados em papel, Módulos de ligação a carboidratos, Domínios-ZZ, Nanopartículas de ouro.

Table of Contents

List of figures

List of tables

List of abbreviations

2DPN	Two dimensional paper network
µPAD	Microfluidic paper-based device
AKD	Alkylketene dimer
AuNP	Gold nanoparticle
BCA	Bicinchoninic Acid
Biotin-AuNP	Gold nanoparticles coated with biotin
BSE	Back-scattered electrons
CBD	Cellulose-binding domains
CBM	Cellulose-binding modules
CBM3	Cellulose binding modules family 3
CipA	Cellulosome-integrating protein A
DNA	Deoxyribonucleic acid
ELISA	Enzyme-linked immunosorbent assay
FITC	Fluorescein isothiocyanate
IgG	Immunoglobulin gamma
IPTG	β-D-1-thiogalactopyranoside
PDMS	Polydimethylsiloxane
SEM	Scanning electron microscopy
SERS	Surface-enhanced Raman spectroscopy
SPR	Surface plasmon resonance

Chapter 1. Introduction

1.1 Microfluidic paper-based analytical devices (μPADs)

Paper has been present in the world of analytical chemistry for centuries, with scientific reports dating back to the early 1800s with litmus paper. But just recently it was rediscovered as a valuable substrate for sensors [1].

Microfluidic paper-based analytical devices (μPADs) are an expanding technology which the invention has been attributed to Whitesides' Group of Harvard University, in 2007 [2]. These systems are characterized by combining some of the capabilities of conventional microfluidic devices with the simplicity of detection methodologies. Basically, μPADs consist in patterning microfluidics channels on paper to guide the flow of aqueous solutions on paper in a desired manner. Besides, it allows multiple tests to be performed on the same platform by creating different reaction zones for different analytes [3].

As a substrate material, paper has many unique advantages: it is made from naturally abundant material cellulose, which is inexpensive and biodegradable; the porous structure allows wicking of liquid, which is important for lateral-flow assays and chromatography applications and so no external power sources are required; paper is suitable for biological applications since cellulose is compatible with biological samples; its surface can be easily manipulated through printing, coating and impregnation and can be fabricated in large quantities; it can be easily stored, transported and disposed, paper properties can be easily altered to suit different applications [3]·[4].

Microfluidic devices using paper as a substrate suggest a path for the development of simple, inexpensive, biodegradable, easy-to-use, portable, disposable platform as low-cost alternatives for health diagnostic, environmental monitoring as well as food quality testing. These systems are designed to handle small volumes and the fluid movement is controlled by capillary action or evaporation, meaning that there is no need for external pumping [2]. Furthermore, the high surface-to volume ratio, porous structure, and the small volume of the paper devices are the reasons for the drastic fall in the time necessary for analysis and for the improvement in the detection limits for colorimetric methods [1]·[5]. Processing of blood samples can be accomplished within 16 min rather than 1 h or overnight as sometimes needed in other methods. Portable enzyme-linked immunosorbent assay (ELISA) provides results in around 40 min, in comparison with traditional methods requiring more than 3 h per assay [5]. Those characteristics make paper a first-choice substrate for disposable sensors.

Currently, paper is used extensively in analytical and clinical chemistry ranging from spot tests for metals [6] and paper chromatography, which has been used to separate and identify mixtures of small molecules, amino acids, proteins, and antibodies [1] to lateral-flow immunoassays, which are largely for paper-based diagnostic assays which can provide a "yes/no" detection of a wide range of analytes using labeled antibodies [7].

1.1.1 Paper structure

Cellulose fibers are the major component of many paper types, with most of the fibers coming from wood. Cellulose is a linear chain macro-molecule composed of hundreds of glucose units. It is fibrous, hydrophilic, biodegradable, and insoluble in water and most organic solvents. Usually cellulose fibers are hollow tubes ~1.5 mm long, 20 µm wide, with a wall thickness of ~2 µm [8]. Some of the most relevant properties of paper are described in table 1.

Table 1-1 Properties of paper (adapted from Nery and Kubota, 2013 [5]).

	Properties	**Impact**
Mechanical properties	Flexibility	Formation of complex 3D structures that do not tear when bent
	High specific stiffness, lightness	
	Thickness	Thickness of tens or hundreds of micrometers results in low (microliter) total volume required for device preparation
	Soft texture	
Fibrous and porous structure	Absorbency	Storage and delivery of an exact volume of reagents inside the paper matrix, which frees the final users from handling chemicals
	Air permeability	Free diffusion of gas throughout the material removes problems usually associated with microfluidic systems—air bubbles
	Network structure	Filtration of the sample, e.g., contaminated with solids, separation of analytes by means of chromatography
	High surface-to-volume ratio	Increase in the number of enzyme molecules or colorimetric probes that can be immobilized
	Capillary action	Ability to wick fluids dispenses with the use of pumps and allows fluid flow in all directions
Natural Origin	Compatible with biological samples	Can increase thermal stability of immobilized molecules, including enzymes and gold nanoparticles
	Disposability and biodegradability	Recyclable, rapidly degraded by microorganisms (~50 days), and easily disposed of by incineration, eliminating the problem of contamination with biological material

Two of the most important macroscopic properties of paper for this type of device are: the thickness, τ (m), and the basis weight, *bw* (g/m^2), which is the mass of dry paper per square meter. The corresponding bulk density of paper can be calculated from the thickness and basis weight according to $\rho_{paper} = bw/\tau$. For example, Whatman No. 1 filter paper, which is the most used type of paper in chemical and analytical assays, has a τ of 180 µm and a *bw* of 87 g/m^2, which translates into a density of ρ_{paper} = 483 kg/m^3 . Since the density of a cellulose fiber is ρ_{fiber} ~1540 kg/m^3 and the paper density corresponds to 483 kg/m^3 the pore fraction of Whatman No.1 paper is around 0.69. Some of the paper's final properties, such as absorptivity, opacity and strength are determined by the porosity which arises from spaces between the fibers, un-collapsed fiber lumens and the intrinsic porosity of the fiber walls [8].

Paper-surface chemistry, controlling contact angle and pore-structure distribution in the paper influence both the rate and the extent of penetration of water. Paper is a very anisotropic material, so

the mass distribution in a paper sheet is usually not constant in the *z* (thickness) dimension. Consequently lateral spreading of fluids in paper is usually more rapid than vertical spreading [8],[9].

These properties of the paper structure have influence in the maximum quantity of biosensor molecules than can be attached to cellulose, which can be estimated by multiplying the maximum density of the immobilized sensor molecules and the specific surface area of the paper structure accessible to the biosensor. Most polymers and proteins immobilized on paper display values in the range 0.1-1 mg/m^2 [8].

1.1.2 Fabrication techniques

Traditional microfluidic devices are fabricated by etching or molding channels into glass, silicone, PDMS, or other polymers or plastics. The possibility of patterning paper provided a new inexpensive and simpler platform for portable assays [10].

The earliest paper-based tests used paper manually cut into sections or strips and treated with a chemical reagent which reacted with an analyte to produce a colored product [1], while the first µPADs were fabricated using photolithography to define flow boundaries, like the one proposed by Whitesides' group [1], [11].

According to the literature, there are a variety of techniques for fabricating paper-based microfluidics devices currently available, namely photolithography [10], [11], plotting with an analogue plotter [12], inkjet etching [13], plasma treatment [14], paper cutting [15], inkjet printing [16], flexography printing [17], screen printing [18], laser treatment [19] and wax printing [9],[20]. The fundamental principle underlying these fabrication techniques (with the exception of the cutting technique) is to pattern a hydrophilic-hydrophobic contrast on a sheet of paper in order to create micron-scale capillary channels on paper. Different techniques use different patterning agents, patterning principles and strategies as shown in Figure 1. The patterning process defines the width and length of the channels, while the thickness of the paper defines the height of the channel [10].

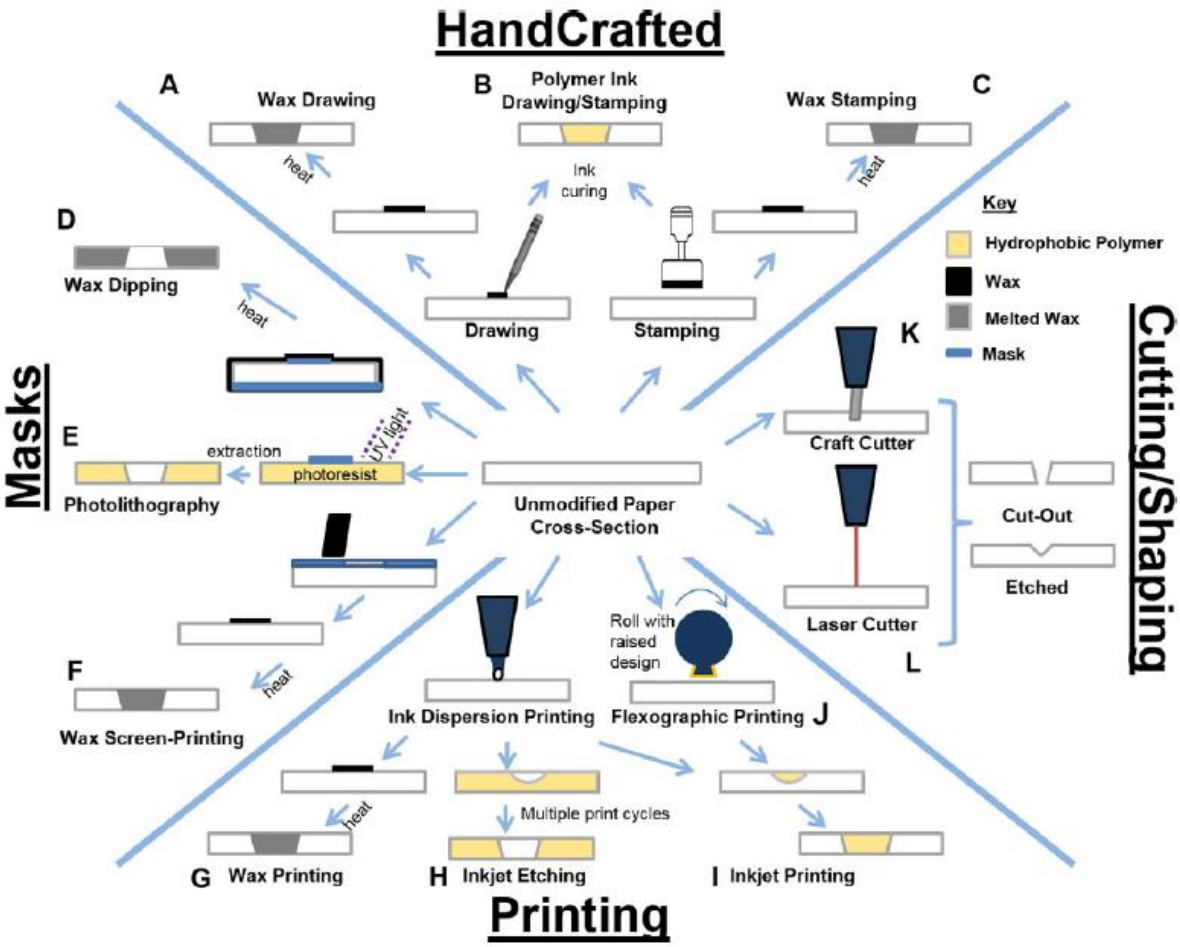

Figure 1-1 Fabrication Schemes for creating µPADs. Hand crafted devices fabricated using (A) Wax drawing, (B) polymer ink drawing or stamping, or (C) wax stamping. Masks were used to protect hydrophilic regions for (D) wax dipping, (E) photolithography, and (F) wax screen-printing. Fabrication techniques with ink addition printers used either (G) wax printing, (H) inkjet etching, (I) inkjet printing, or (J) flexographic printing. Cutting or shaping air boundaries or etching channels were performed by a (K) craft cutter or (L) laser cutter. From [1].

The fabrication method for µPADs can be tuned to fulfill the needs of the end-user, depending on the goal to be achieved. Therefore, to choose the proper technique, it is necessary to consider a range of factors including material costs, fabrication process simplicity and the intended applications of paper-based microfluidics devices [1]·[2]. The advantages and limitations of each fabrication technique are listed in Table 1-2.

Table 1-2 Description of the patterning agent, main advantages and drawbacks for the different fabrication techniques of paper-based microfluidic devices. Adapted from [1],[2],[5].

Fabrication technique	**Patterning agent**	**Advantages**	**Drawbacks**
Photolithography	Photoresist	High resolution of microfluidic channels (channel width is as narrow as 200 μm)	Requires expensive equipment; Requires an extra washing step to remove un-crosslinked polymer; Devices are vulnerable to bending
Plotting	PDMS	Hydrophilic channels not exposed to polymers or solvents; Hydrophobic barriers are flexible; Patterning agent is cheap	Requires a customized plotter; Cannot be readily applied to high throughput production
Inkjet etching	Polystyrene	Reagents can be inkjet into the test zones using the printer	Requires a customized inkjet printer; Not suitable for mass fabrication; Hydrophilic areas exposed to polymers or solvents
Plasma treatment	AKD	Uses very cheap patterning agent	Hydrophilic areas exposed to polymers or solvents; Metal masks must be made for each pattern; Cannot produce arrays of free-standing hydrophobic patterns
Wax printing	Wax	Rapid (~5 minutes); Requires only a commercial printer and hot plate; Hydrophilic channels not exposed to polymers or solvents	The design of the patterns must account for the spreading of the wax in the paper; Extra heating step required after wax deposition
Inkjet printing	AKD	Uses very cheap AKD Produces massive devices fast (<10 min) and simply; Requires only a desktop printer	Requires an extra heating step after AKD deposition; Requires modified ink jet printers
Flexography printing	Polystyrene	Allows direct roll-to-roll production in existing printing houses; Avoids the heat treatment of printed patterns Low ink usage	Requires two prints of polystyrene solution and different printing plates; Print quality relies on the paper surface
Screen printing	Wax	Simple process	Low resolution of microfluidics channels; Requires different printing screens for creating different patterns
Laser treatment	Depend on paper types	High resolution (minimum pattern size of about 62 μm)	Microfluidic channels do not allow lateral flow of fluids; Requires extra coating for liquid flow

At present, AKD ink jet printing and wax printing might be the most promising techniques due to the low cost of patterning agents and easy, rapid fabrication process; both techniques can produce multiple devices in a piece of A4-sized paper within 10 min with a single print-and-heat cycle [2].

The fabrication of paper-based microfluidic devices by wax printing was introduced by Lu *et al.* [20] and Carrilho *et al*. [9] and consists in only two steps: i) the patterning of hydrophobic barriers of wax using a commercially available printer and ii) the heating of the paper to melt the wax, which thus penetrates the paper and generates a complete hydrophobic barrier. Since paper is an anisotropic material, the lateral spreading of wax is faster than the vertical spreading. This complicates the design of the channels, because the dimensions of the printer pattern will not correspond exactly to the dimensions of the resulting hydrophobic barriers. Considering this, Carrilho *et al.* [9] studied the spreading of molten wax in paper (Whatman No. 1 chromatography paper) to correlate the width of the hydrophobic barrier after melted, with the width of the initial pattern in order to simplify the production of a paper-based device. They realized that the spreading of molten wax in paper is a process of capillary flow in porous materials, which can be described by Washburn's equation [21]:

$$\boldsymbol{L = (\gamma D\, t/4\eta)^{1/2}} \qquad (1)$$

where *L* stands for the distance that a liquid of viscosity η and surface tension *Y* penetrates into a porous material with an average pore diameter *D*, in time *t*.

The viscosity of the wax depends on the temperature, so it is important to ensure the use of a uniform and well-controlled heat source for reproducible results. Assuming that the rest of the parameters of the equation 1 are kept constant, the final width of the hydrophobic barriers depends mainly on the width initially printed on paper. This relation is described by the following equation [9]

$$\boldsymbol{W_B = W_P + 2L} \qquad (2)$$

where W_B represents the width of the barrier, W_P is the width of the printed line, and *L*, which can be determined experimentally, corresponds to the distance that the wax spreads from the edge of the printed line in a direction perpendicular to the line (See Figure 1-2).

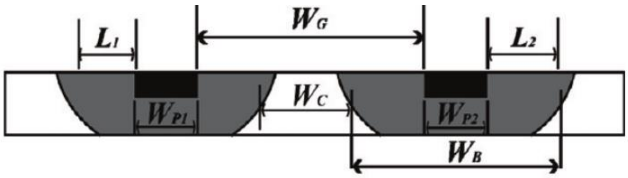

Figure 1-2 Schematic representation of the spreading of molten wax in paper with the variables to take in account for rational design of µPAD. W_P - width of the printed line; W_G - separation between the edge of the lines before melting; W_B - thickness of the hydrophobic barrier defined as the middle point between the front and back widths (average width); W_C - width of the resulting channel after melting of the wax; L - spreading of the wax in relation to the original edge of the line. The black rectangles represent the wax before the heating step while the grey area represents the wax after the heating step. Adapted from [9].

The width of a hydrophilic channel defined by two parallel hydrophobic barriers can be determined by [9]:

$$\boldsymbol{W_C = W_G + 2L} \qquad (2)$$

where W_C is the width of the hydrophilic channel and W_G is the space between the two printed lines (also in micrometers), measured on the edge of the line.

Despite a small loss in resolution, there are many advantages to wax printing. The hydrophilic channels are never exposed to solvents or polymers, existing commercial wax printers are readily available at a relatively low cost, and the process is rapid (~5 min) and simple.

Although many devices fabricated for research and proof of concept purposes are simply open channel and testing zones, sometimes it is necessary to consider packaging the devices. Sealing the devices, especially when reagents are stored in paper prevents device contamination and allows long-term storage. Sealing has also been used to minimize or control solvent evaporation within devices, which can increase detection sensitivity. Although adding plastic packaging increases the device cost, it also has the advantage of providing physical support and keeps the devices more mechanically stable [1],[22].

1.1.3 Biosensors and bioactive paper

A biosensor is generally defined as a device comprising a biological recognition system (or bioreceptor), and a transducer. The analyte in study reacts with the bioreceptor and produces an effect measured by the transducer, which converts it in a measurable effect [23]. Therefore, after µPAD fabrication, it is necessary to add a bioreceptor agent, which can be enzymes, antibodies, DNA, aptamers and synthetic polymers[4]. The immobilization of biomolecules on paper is influenced by its structure and chemistry. The structure of paper influences the maximum quantity of bioreceptor molecules that can be attached to cellulose, while the surface chemistry must facilitate bioreceptor immobilization, minimize non-specific adsorption and be compatible with reporting strategies [4]. The immobilization strategies used for bioreceptors can be divided in: physical immobilization, chemical immobilization and bioaffinity attachment [4].

The most used strategy is physical immobilization, which is a simple method for coating surfaces, since it does not require modification of the biomolecule or surface. It takes advantage of non-covalent interactions such as van der Waals forces, hydrogen bonding, and hydrophobic interactions. The adsorbed molecules form a randomly oriented, heterogeneous surface, which may lead to reduced activity. Furthermore, the surface density is not always very high [4].

Chemical immobilization relies on covalent binding and it is the most stable and uniform immobilization on a paper. To covalently link biomolecules onto paper, both the biomolecules and the paper need to contain functional chemical groups through which the immobilization occurs. Cellulose has few of those groups, so activation with a polymer or a small molecule is essential to add surface functional groups suitable for a subsequent bioconjugation reaction [4].

Bioaffinity attachment or biochemical coupling attachment occurs via bioaffinity interactions between the matrix/ligand and a biomolecule. In this case the orientation of the immobilized biomolecule is controlled ensuring full biological activity and stability [4]. One example is the carbohydrate binding-

module (CBM), which is a protein with high affinity to cellulose and can be engineered and fused with proteins or antibodies [24]·[25].

1.1.4 Incorporating functionality

Paper is an exceptional substrate for controlling fluid flow without external power and for confining liquids to specified regions. Unfortunately, the physical properties inherent to porous substrates offer limited control over fluid transport, especially regarding the rate and direction of flow. This renders many paper-based methods ill-suited for handling complex chemical matrixes or for performing multistep tasks. The earliest μPADs were incapable of complex functionality, limiting their impact in the analytical community. More recently, research groups have begun integrating functionality into μPADs for better liquid handling and autonomous operation within the device, opening new opportunities for μPADs as a viable alternative to traditional analytical methods [1].

1.1.4.1 Programing and timing

One of the first demonstrations for controlling complex fluid flow was in 2010 by Martinez et al. [26] with the development of a three-dimensional μPAD incorporating single-use “on” buttons designed to direct the flow path. Strategically positioned gaps separated layers of paper and tape and then connected fluidic paths when pressed. This digital valve was capable of preventing flow completely until pressed (Figure 1-3). Single-use valves have limitations, but this work demonstrated the utility of programmable μPADs for prioritizing sample testing or for manually controlling timed reaction sequences.

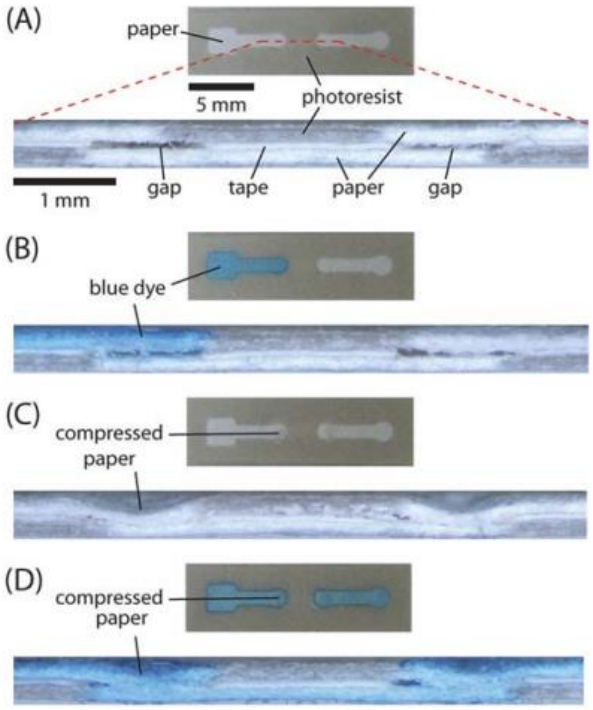

Figure 1-3 Demonstration of ‘on’ buttons. (A) Top view and cross-section of a fully assembled 3-D device. The cross-section shows the two layers of paper, the layer of tape, and the small gaps between the channels. The cross-

section image is obtained by sectioning the device, as illustrated by dashed line. (B) Top view and cross-section of a device identical to the one shown in (A) after adding 10 mL aqueous blue dye to the left end of the channel. The gaps prevented the dye from wicking between the two adjacent layers of paper. (C) Top view and cross-section of a 3-D device after closing the gaps by compressing the top layer of paper with a ballpoint pen. (D) Top view and cross-section of a device identical to the one shown in (C) after adding blue dye to the left end of the channel. The dye wicked across the entire length of the channel. Adapted from [26].

There are additional methods for controlling fluidic transport, primarily by changing the channel geometry. Channel junctions that transition from narrow to wide experience a reduction in flow rate [27]. Toley *et al.* [28] introduced another method for controlling flow by diverting it through a tunable cellulosic shunt placed in the flow path and in complete contact with the nitrocellulose substrate (Figure 1-4A). By tuning the length, width, and thickness of a shunt, the authors reported that flow could be delayed from 3 to 20 min with coefficients of variation under 10% [28].

Another method demonstrated is fluidic barriers made of materials soluble in the carrier fluid, like sucrose, which is a common material for these barriers because it is inexpensive and readily abundant. This concept was applied by Houghtaling *et al.*, who developed a digital "on/off" switch in which a bridge composed of soluble sugars (mannose or trehalose) wicks fluid through it until eventually dissolving and effectively shutting off flow completely (Figure 1-4B). The bridge material concentration and/or geometry can be tuned for the desired effect [29].

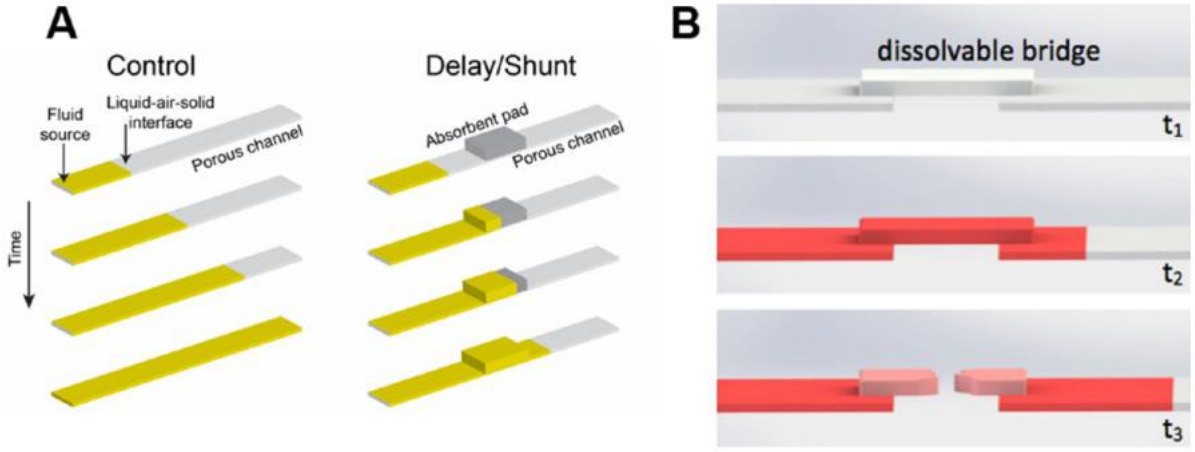

Figure 1-4 A) Tunable paper shunts delay fluid flow by controlling shunt width, height, and placement in the porous channel. **B)** A dissolvable bridge functions as a digital "on/off" switch. Once the bridge dissolves in the carrier fluid, flow ceases. Adapted from [1]·[28]·[29].

Another approach to paper-based valves is to build 2D microfluidic networks with programmable fluidic disconnects [22]. The assay employs multiple converging fluid inlets to control the arrival time of each fluid to a detection zone. The system comprises of a fluidic network and a fluid reservoir to allow programmed disconnection of fluid sources, required for multi-step delivery. The 2D microfluidic network

has legs with different lengths and the legs are immersed in the fluid reservoir. As the fluid level drops, the legs disconnect in their order of length and programmable sequence.

1.1.4.2 Three dimensional systems

Fabrication of µPADs with multiple layers to form three-dimensional (3D) devices has been of interest because functionality can be added without increasing device size[1]. Three-dimensional µPADs offer several potential advantages over 2D devices. They are advantageous for certain applications because they: accommodate more assays on the same footprint of a device than a 2D device; enable fluid movement in three dimensions through multiple layers of paper, which opens the potential for multi-step assays in a compact device; and move fluid through the thickness of paper (the z-direction) and laterally (the x-,y-plane). This latter characteristic minimizes the quantity of sample that is lost in swelling the paper, increases distribution times and decreases the necessary sample volume for an assay [27].

The 3D µPAD shown in Figure 1-5 was able to assay in duplicate up to four different samples for glucose and protein. The test zones were arranged in a side-by-side configuration for easy comparison of the results. The device was designed to incorporate a fluid inlet at the corner of the device, so that the device could be dipped into a drop of each sample [10].

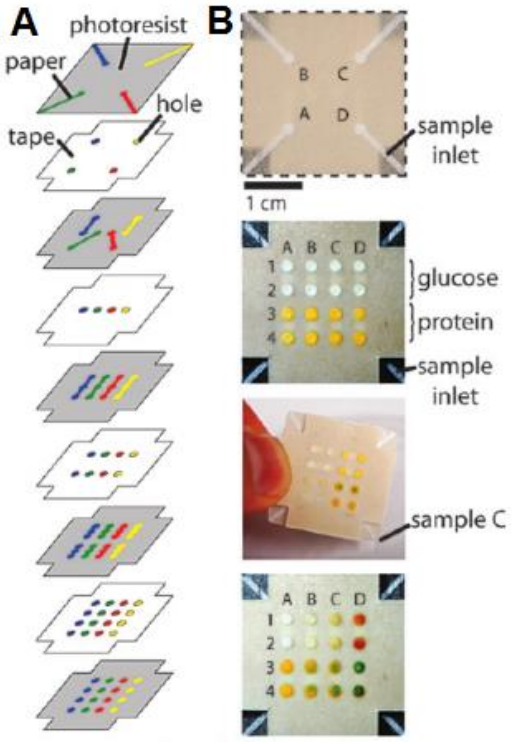

Figure 1-5 - A) Schematic representation of the layers of paper and tape used to assemble a device designed for testing four samples for the presence of glucose and protein. **B)** Three-dimensional µPAD that can test four different samples for glucose and protein. The front face of the device has four fluid inlets at each corner of the device that can be dipped directly into the sample. The back face of the device has an array of 16 test zones that were pre-spotted with the reagents for the assays. The results of the assays are displayed side by side for easy comparison. Adapted from [10]

1.1.4.3 Multistep processing

The trend toward increasing the functionality of μPAD assays starts with automating multistep processes. Multi-step chemical processing sequences can be useful in sample pretreatment. 2D microfluidic networks can be configured to have multiple inlets per outlet to enable controlled transportation of reagents within a single device. This process can be accomplished by modifying the geometry of the network. Sequential reagent delivery was demonstrated by constructing a nitrocellulose-based network comprising of three staggered inlets, which lead to a common segment of the body. When increasing volumes of reagents were wicked up by the segregated channels, the fluid with the shortest path reaches the detection region first, followed by the fluids from medium and longest inlets [22], [27] (Figure 1-6).

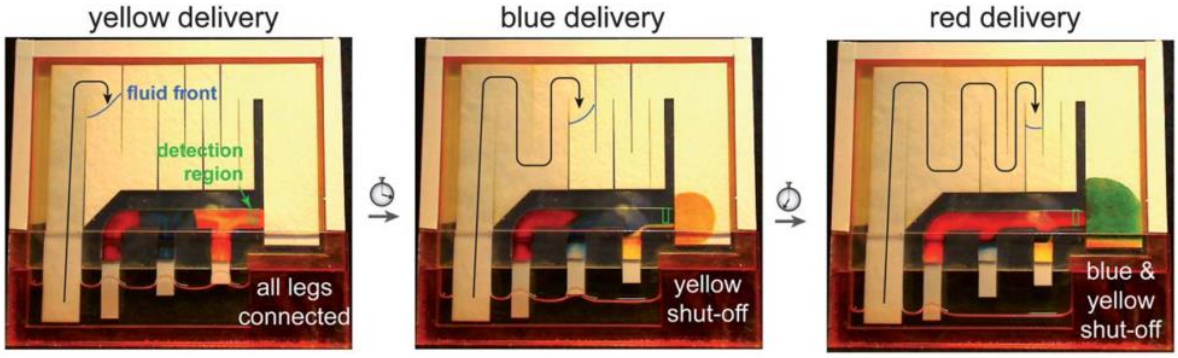

Figure 1-6 Autonomous fluid delivery in a 2DPN. Each leg wicked fluid from a single buffer source, and dried dyes representing reagents create different fluids from each leg (colours). Each coloured fluid arrived at a different time at the ‘‘detection zone’’ (green box) and was shut off in a timed sequence after delivery. Adapted from [22]

To improve the portability, utility, and user-friendliness of μPADs, any necessary reagents can be included on the device, preferably in a dry state. This has several benefits associated: (1) the number of required user steps is reduced, (2) the complexity of shipping test kits is reduced because dry reagents are contained within the paper network, and (3) dry reagents are less labile in changing environmental conditions [1].

1.1.4.4 Surface Chemistry

The components of paper can be tailored to meet certain required quality demands. Paper can be functionalized at different levels of the manufacturing process. Functional chemicals can be added to the paper during and after the web formation, and functional components can be added to the finished paper product during the paper-making conversion processes or can be printed on the surface of the paper [4]. Altering the surface chemistry of paper is an effective technique for controlling fluid flow, improving color uniformity and enhancing chemical stability.

Once fully wetted, paper tends to lose much of its functionality for driving fluid transport. To address this limitation, Gong *et al.* coupled a nanoporous membrane with ion concentration polarization to concentrate analytes and maintain fluidic transport even in fully saturated channels [30].

1.1.5 Detection techniques used in µPADs

One critical step for µPADs is the ability to detect and quantify an analyte. The most common analytical detection technique for µPADs is colorimetry because analysis is relatively simple (i.e., color intensity is proportional to analyte concentration), and the technology is compatible with smartphone-based reporting systems.

In general, four detection methods have been reported for the detection of analytes in paper-based microfluidics: colorimetric detection, electrochemical detection, chemiluminescence detection, and fluorescence detection.

Colorimetric detection chemistries are typically related to enzymatic or chemical color-change reactions. In most cases, the analysis of results can be visually assessed by the unaided eye, which is adequate when a yes/no answer or a semi-quantitative detection is sufficient for diagnosis. Molecular and enzymatic dyes represent the simplest and most used method for detection. Colorimetric sensing can produce semi-quantitative readouts with the help of a calibration chart. In paper-based microfluidic devices, multiple detection zones are employed to capture different analytes within the same device. After the fabrication of hydrophobic patterns in paper, detection zones can be formed by spotting reagents in the detection zones. In such multiplex assays, an enzymatic or a chemical reaction between the target analyte in the sample and immobilized reagents take place. These reagents can be enzymes, acid–base indicators or dyes. Early examples of colorimetric sensing in paper-based microfluidics were demonstrated using glucose in artificial urine. When a sample was introduced in the paper-based microfluidic device, it was distributed into the reaction zones, yielding a color change and enabling visual determination of analyte levels using a calibration chart. In the glucose assay, the positive result was recorded when the color shifted from clear to brown, based on the enzymatic oxidation of iodide to iodine [27].

Electrochemical detection has been exploited widely due to its maturity and well-understood working principles. Usually, electrochemical sensors encompass three electrodes: a counter electrode, a working electrode and one or multiple reference electrodes. Carbon inks are well-known materials used in the fabrication of counter and working electrodes, whereas silver/silver chloride ink is used for the fabrication of reference electrodes. In contrast to colorimetric sensing, electrochemical sensing has demonstrated fast sensor responses and higher sensitivities, down to nM ranges. Electrochemical detection is also independent of the ambient light and is less prone to interference from the color/deteriorations of paper, but requires reading equipment.

Chemiluminescense, is based on the emission of light generated by a chemical reaction. One example is the reaction is hydrogen peroxidase catalyses the oxidation of luminol to 3-aminophthalate

and the decay of the excited state, to a lower energy level results in light emission. This technique has been exploited, in paper-based microfluidics, for detection of tumor marker besides other biological analytes. Studies on the detection of tumor markers involved building sandwich-type immunoassays with a typical luminol-H_2O_2 chemiluminescence system and catalyzed by Ag nanoparticles [5],[27]. This is a simple, low cost and highly sensitive method, which measurement may be performed in the dark.

Fluorescence detection is highly sensitive, but requires instrumentation for signal detection. In addition, the use of optical brightening agents to turn commercial paper white confers paper a slight fluorescence, resulting in high background signal [8]. The feasibility of fluorescence sensing will be dependent on the advances in cost reduction and miniaturization of fluorescence readers [27].

A unique selling point of lateral flow assays has been their lack of requirement for readout devices over the last decades. During early years of lateral flow assay development, manufacturers focused on cost and the ability to deliver a yes/no answer. This attractive attribute combined with low-cost, mobility and easy-to-read factors are the reasons for their popularity, but nowadays, the focus of paper-based assays is shifting towards a more sensitive and quantification-able system. Nevertheless they still require a trained healthcare provider to interpret the data they provide and to prescribe any necessary treatment. For this reason, telemedicine is an attractive alternative system for developing countries [2],[31]. Using this approach, the result obtained can be photographed by a camera on a mobile phone and then sent to a remote location where an expert analyzes the image and prescribes an appropriate treatment.

1.1.5.1 Gold nanoparticles as a colorimetric reporting agent

Gold nanoparticles (AuNPs) are one of the most extensively studied nanomaterials. The first report of gold colloids was published more than 100 years ago by Faraday [32]. Since then, numerous studies have been reported on the synthesis, properties and applications of gold clusters, colloids, and nanoparticles [33], [34]. Gold nanoparticles exhibit many unique and interesting physical and optical properties such as surface plasmon resonance (SPR), surface enhanced Raman scattering (SERS), and quantized charging effect [33], [34]. The surface plasmon resonance of gold nanoparticles is an optical property that holds potential in biosensing, molecular imaging, and photo-thermal treatment of diseases. Mirkin *et al*. [35] and Zhao *et al.* [36] demonstrated the use of gold nanoparticles as an optical probe to detect DNA molecules based on the color change of individually scattered nanoparticles and the complementary DNA-hybridized nanoparticle aggregates.

Among the conventional methods of synthesis of AuNPs by reduction of gold(III) derivatives, the most popular one for a long time has been the Turkevitch method, which consists in the citrate reduction of $HAuCl_4$ in water [37]. This method leads to AuNPs of 15 to 20 nm. In 1973 Frens reported to obtain AuNPs of pre-chosen size (between 16 and 147 nm) via their controlled formation, by manipulating the ratio between the reducing/stabilizing agents (the trisodium citrate-to-gold ratio) [38].

AuNPs are the most stable metal nanoparticles, presenting fascinating aspects such as their assembly of multiple types involving materials science, the behavior of the individual particles, size-

related electronic, magnetic and optical properties (quantum size effect), and their applications to catalysis and biology [34]. They are very versatile molecules being possible to functionalize their surface with the most diverse ligands depending on its purpose.

AuNPs have already been used in a variety of dipsticks and lateral flow tests coupled with antibodies, since they are easy to synthesize and manipulate, stable in time, size-tunable, biocompatible and have an intense red color easy to be detected even by naked eye or usually using color readers to achieve better detection limits [39].

1.1.6 Applications of µPADs

The main application of paper-based microfluidic devices is to provide a low-cost, easy-to-use, and portable analytical platform for assays, either multi-analyte or semi-quantitative (even quantitative), across a range of application areas such as in health diagnostics, environmental monitoring and food quality control. Researchers have focused on developing these simple and inexpensive paper-based sensors so they can be used in the developing world where a fast and simple diagnostic is highly desirable [2]·[40].

To date, several studies involving µPADs have been conducted using real samples such as urine, saliva and blood for detection of various types of analytes with clinical relevance. One important mark was the first µPAD published by Whitesides' group [11], which was able to detect multiple samples in parallel and in a relatively short period of time onto the same device. It allows the simultaneous, visual detection of glucose and protein in an artificial urine sample (Figure 6). Glucose assay is based on the enzymatic oxidation of iodide to iodine, in which the presence of glucose results is a color change to brown. On the other hand, a positive result in the protein assay is based on a color change of tetrabromophenol blue from yellow to blue.

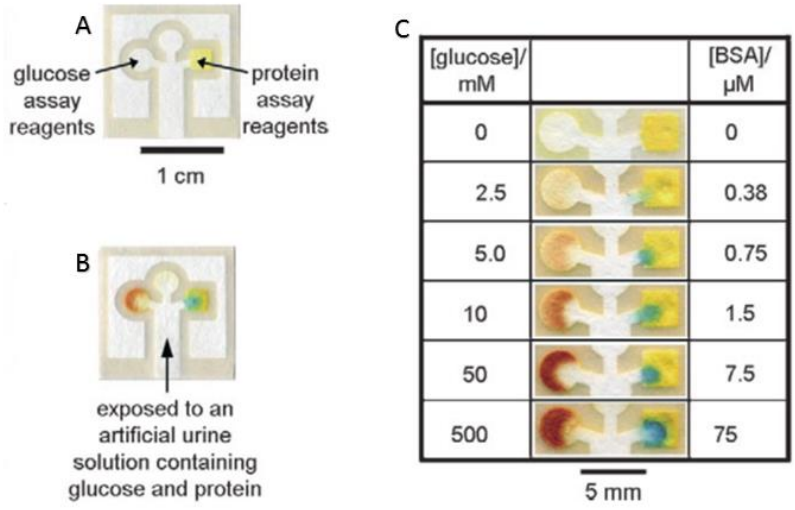

Figure 1-7 A) Chromatography paper patterned with photoresist. The square region on the right is the protein test and the circular region on the left is the glucose test; **B)** Positive assay for glucose (left) and protein (right); **C)** Glucose and protein detection assays by using varying concentrations of glucose and BSA. Adapted from [11].

In the diagnosis of diseases, early detection is essential for the treatment to be successful. By using cheap, paper-based microfluidic devices, it makes diagnosis accessible to all, and for a rapid result to be obtained with facile device operation. An example of this application is described by Ge *et al.* [41]. Based on the simple and well established concept of paper folding, the group has shown that chemiluminescence detection of four cancer biomarkers in whole blood samples can be performed in a single run without the need for multiple washing steps.

Khan *et al.* [42] developed a low cost blood sensor to detect blood type, based in the agglutination of red blood cells upon interaction with immunoglobin M antibodies. The wicking ability and transport of sample, in a paper substrate, could be used as an indicator of agglutination.

Paper-based approaches for environmental monitoring are attractive because accurate, low-cost monitoring is pivotal for environmental applications where routine testing is performed, such as for the analysis of river/soil contamination, occupational exposures, or air pollution. Many colorimetric µPADs have been developed for metal detection because of their known toxicity. Environmental metal contamination is common in three sources, air (aerosols), water, and soil. One of the first examples of µPAD-based quantification of metals was a sensor comprised of four detection zones for simultaneously measuring Fe, Cu, and Ni from combustion ash [6]. Aerosolized metals were collected on filters and transferred to a µPAD that had been treated with chromogenic reagents. Detection limits ranged from 1 to 1.5 µg (total mass) for each metal analyte [1]. Apilux *et al.* [43] developed a fast, simple and portable dual electrochemical/colorimetric paper-based system for detecting gold and iron. The recovery of gold from industrial waste is important due to its high economic value, whereas iron is common for interfering in the analysis. Gold was detected down to 1 ppm by square wave voltammetry in a diluted aqua regia solution, whereas iron which interferes electrochemically with its analysis was monitored colorimetrically [40].

Paper-based devices have been proposed as a preventive detection method to provide simple, low-cost, and on-site detection of foodborne contaminants. µPAD devices developed for bacteria detection in food have relied primarily on enzymatic activity or immunoassays for detection. Hossain *et al.* [44] studied the detection of pesticides in beverages and food samples. The sensor consisted acetylcholinesterase enzyme and iodophenyl acetate reagent for the assay where the combination of the two created a blue color. The presence of pesticides was indicated by a decrease in the blue color intensity, which was interpreted using a digital camera. Even though additional processing using a computer was needed, it still was simple and fast when compared with other laboratory tests [40].

1.2 Carbohydrate-binding modules

Cellulose is the main polysaccharide component of the plant cell wall and is degraded in nature into simple soluble sugars by bacterial and fungal enzymes. The degradation of cellulose became a theme of interest for researchers due to its insoluble nature and inherent stability, which constitutes a challenge for enzymatic hydrolysis [45].

The enzymatic degradation of insoluble polysaccharides by glycoside hydrolases is relatively inefficient, because target glycosidic bonds are often inaccessible to the active site of these enzymes. To overcome this, many glycoside hydrolases are modular, comprising catalytic and non-catalytic sugar binding modules, which includes carbohydrate binding modules (CBMs) [46]. A CBM is defined as a contiguous amino acid sequence within a carbohydrate-active enzyme with carbohydrate binding activity, which facilitates the binding of hydrolytic enzymes to cellulose, enhancing its degradation [46], [47]. CBMs were initially defined as CBDs (cellulose-binding domains), based on the initial discovery of several modules that bound cellulose [48]. However, throughout the years additional modules have been reported having a diverse ligand specificity, so the term CBM (carbohydrate-binding module) was proposed as a more inclusive term to describe all of the non-catalytic sugar-binding modules derived from glycoside hydrolases [46].

Many organisms produce different CBMs. To date, CBMs can be classified into 71 different families, depending on specific characteristics such as the amino acid sequence, binding specificity and structure [49]. They range in size from only about 40 to approximately 200 amino acid residues [50]. Structural and functional studies on representatives of the majority of CBM families show that the topology of CBM ligand-binding sites complements the conformation of the target polysaccharide. Based in these structural and functional similarities, CBMs families have been grouped in three types. Type A CBMs interact with the flat surfaces of crystalline polysaccharides, primarily cellulose. Their bind sites comprise a planar hydrophobic platform rich in aromatic amino acids residues. Type B modules can bind to the internal regions of single glycan chains. Type C CBMs recognize small saccharides containing from one to three monosaccharide units or, in the context of complex polysaccharides, the termini of these polymers [46], [51].

Many applications have been reported on the use of the high stability binding of CBMs to cellulosic surfaces. CBMs can be combined with other biomolecules such as proteins, antibodies and even cells [52]–[54]. The first commercial application was the use of CBMs in fusion proteins as tags for affinity purification or immobilization. Since CBMs adsorb spontaneously to cellulose, no pretreatment of the samples is required prior to the immobilization [25]. Such CBM-based constructs offer the possibility for targeted immobilization of biomolecules onto a cellulose matrix for fiber modification, protein purification, diagnostics, or bacterial adhesion [55]–[57].

1.2.1 Carbohydrate binding module family 3

Cellulosomes are multi-enzyme complexes, which act synergistically with various enzymes in order to hydrolyze the crystalline cellulose and polysaccharides in plant cell walls. In nature, these complexes have been identified in certain anaerobes, which include the *Clostridium* bacterium strain, such as *Clostridium thermocellum.* This gram-positive thermophilic bacterium is highly efficient in the production of one of the most efficient enzymatic cellulose degradation systems [58].

The *C. thermocellum* cellulosome has a structural multi-domain protein called CipA (cellulosome-integrating protein A), which consists of a single large polypeptide chain with 197 kDa that

includes different subunits with different functions [59]. CipA includes nine enzyme-binding cohesin modules, which interact with the dockerin modules present in the catalytic subunits, in order to promote the integration and assembly of the hydrolytic enzymes into a complex cellulosome structure [51]. A C-terminal divergent dockerin present in the scaffoldins targets the cellulosome to the bacterial cell envelope. The entire complex is anchored to cellulose via a CBM3 that is also present in the scaffoldins [58]. CBM3 is located between the cohesin 2 and cohesion 3 and is flanked by two linker regions rich in threonine and proline residues. The linker segments of peptide have sufficient length and flexibility to allow the efficient orientation and operation of the catalytic site making polysaccharide degradation more efficient [60].

The Carbohydrate-Binding Module 3 (CBM3) has 155 residues and is classified as a type A CBM, which binds tightly to the surface of crystalline cellulose. This CBM mediates the primary recognition and binding of the scaffoldin subunit, along with its attached cellulosomal enzymes, to the cellulosic substrate. When the cellulosome complex is implanted, the CipA CBM mediates the binding of the entire cell to the insoluble substrate. The 3D crystal structure of CBM3 from the *C. thermocellum* CipA scaffoldin is mainly based on nine β strands arranged in two antiparallel sheets and connecting loops [61].

CBM3 can be conjugated with other biomolecules, through fusion-protein technology, resulting in a molecule with a bioactive domain and a binding domain with a high affinity to cellulose. Rosa *et al*. [24] described the use of a CBM3 fused with a double-Z fragment of the staphylococcal protein A as an affinity immobilization technique to develop a wax printed μPAD for molecular diagnostics of infectious diseases. Antibodies immobilized through biochemical coupling were able to capture labeled-DNA strands and hybridized DNA using an FITC-labeled-DNA probe more efficiently than the ones immobilized by physical adsorption. This strategy increased substantially the efficiency of the μPAD, since it minimized the loss of antibodies during the preparation steps, resulting in a higher intensity and spatial confinement of the signals.

Chapter 2. Objectives

The main objective of this work is to evaluate, through proof-of-concept experiments, the possibility of developing microfluidic paper-based analytical devices (μPAD) for immunodetection which use gold nanoparticles as a colorimetric detection method and the CBM3-ZZ fusion protein as an intermediate for antibody immobilization. The CBM3-ZZ fusion protein combines the cellulose binding properties of CBM3a from *C*. *thermocellum* CipA scaffoldin with the antibody-binding properties of a double Z-domain from the staphylococcal protein A.

The first goal of the work is to compare the ability of an anti-biotin IgG, immobilized on paper either through biochemical coupling with CBM3-ZZ or through physical adsorption, to capture gold nanoparticles coated with biotin. Experiments are performed both in 4 mm circular reaction areas (spots) and in closed microfluidic channels fabricated by wax-printing, a technique that is used to delineate hydrophobic barriers on paper. The capture of the gold nanoparticles by the antibiotin IgG is assessed by observing the generation of a red color due to the accumulation of the gold nanoparticles in the surface of the reaction zone. Several assays comparing both immobilization techniques in either of the designed paper-based analytical devices, such as optimization of the gold nanoparticles deposition, analytical performance and rehydration are made.

Chapter 3. Materials and Methods

3.1 Antibodies

FITC-Human IgG was obtained from Sigma-Aldrich (St. Louis, MO). Mouse monoclonal anti-FITC (IgG2a isotype) and mouse monoclonal antibiotin (IgG2a) were obtained from Abcam (Cambridge, UK). Species and antibody class were chosen based on their strong binding to protein A.

3.2 Nanoparticles

InnovaCoat™ Gold Biotin-40 nm (OD 10.0) was obtained from Innova Biosciences (Cambridge, UK). Through this work the biotin labeled gold nanoparticles will be mentioned as Biotin-AuNPs.

3.3 Paper analytical device fabrication

All assays using paper were performed in Whatman no. 1 chromatography paper, which is available in 25 x 25 cm sheets (catalog number: 3001-878; Whatman™, GE Healthcare©, Buckinghamshire, UK). This paper is hydrophilic, homogeneous, biocompatible, readily available, relatively inexpensive, and has a thickness of 0.18 mm [9]. After cutting to the desired size, these sheets can be fed directly into the printer. Patterns of hydrophobic barriers were designed as black lines on a white background using drawing software (AutoCAD).

The wax printing method was used to pattern hydrophobic barriers onto Whatman No.1 chromatography paper. A Xerox ColorQube 8570 color printer was used to print wax-based inks. The print head dispenses ink (melted wax) on the surface of the paper, where it cools and solidifies instantaneously without further spreading. The ink contains hydrophobic carbamates, hydrocarbons, and dyes that melt around 120 ºC. The default printer parameters were used for enhanced resolution printing. Two designs of patterned paper devices were used, 4 mm diameter circles with 0.4 mm line thickness (referred as spots from now on), and microfluidic channels of 2.4 mm nominal width and 28 mm nominal length (plus a reservoir of 13 mm nominal length), defined by lines of 0.4 mm nominal thickness. After printed, the paper devices are heated on a magnetic stirrer/heat plate with temperature sensor (MR Hei-Standard, Heidolph Instruments©, Schwabach, Germany) with temperature set at 150 ºC for 2 minutes. In this step it is important to use a flat and uniformly heating surface to create a uniform three-dimensional hydrophobic barrier[9]. The paper device is ready to use after cooling at room temperature.

3.4 Production of CBM3-ZZ

The CBM3-ZZ fusion protein (~30 kDa) was cloned in *E. coli* by NZYTech, Lda.. The fusion combines an N-terminal double Z-domain of the staphylococcal protein A and the family 3 cellulose-binding module from *C. thermocellum* CipA. The genes were cloned into the NdeI-XhoI sites of a pET21a

(Novagen) expression vector. The corresponding pET_ZZCBM3 plasmid was used to transform the *E. coli* DE3 strain BL21 (Novagen). The amino acid sequence of the CBM3-ZZ fusion protein is shown in Figure 3-1.

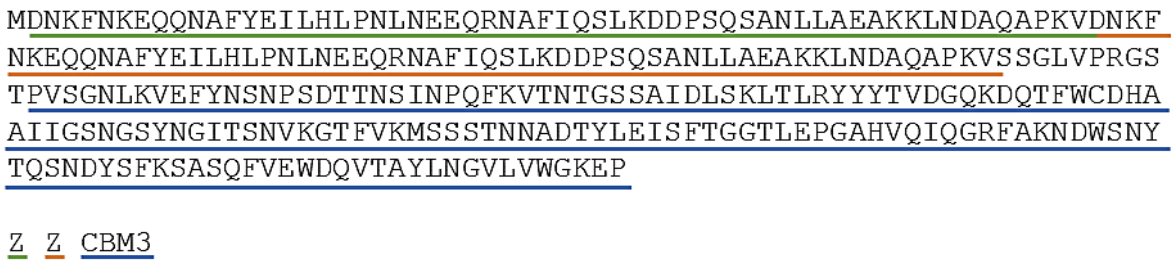

Figure 3-1 Amino acid sequence of the CBM3-ZZ fusion protein.

Liquid LB media (Luria Bertani Broth, Miller) containing 10 g/L casein enzymatic hydrolysate, 5 g/L yeast extract and 10 g/L sodium chloride (pH 7.5 ± 0.2 at 25 ºC) was prepared according to the manufacturer's specifications.

For CBM3-ZZ production, 100 µL of *E. coli* DE3 strain BL21 transformed with pET_ZZCBM3 were cultivated in 5 mL of LB media supplemented with 100 µg/mL ampicillin. Cells were cultured overnight at 37 ºC with a shaking rate of 250 rpm. After reading the $OD_{600\ nm}$, the cell suspension was diluted down to an $OD_{600\ nm}$ of 0.1 and used to inoculate 250 mL of LB media supplemented with 100 µg/mL ampicillin. Cells were grown at 37 ºC with a shaking rate of 250 rpm and expression was induced at an $OD_{550\ nm}$ of ~0.5 with 1 mM isopropyl β-D-1-thiogalactopyranoside (IPTG) for 16 hours at 37 ºC (250 rpm). Cells were harvested by centrifugation at 1900 g (Sorvall® RC-6 Plus superspeed centrifuge with SS34 rotor), 4 ºC, for 10 minutes, and ressuspended in a minimum volume of Tris-saline Tween 20 buffer (TST: 50 mM Tris buffer, pH 7.6, 150 mM NaCl, 0.05% Tween 20). Cells were disrupted by sonication (Branson Sonifier 250) for 6 x 30 seconds on ice with interruptions of 30 seconds (50% duty cycle, microtip limit 5). Centrifugation at 12,000 g, at room temperature, for 20 minutes was performed to separate the supernatant containing the fusion protein from cell debris.

3.5 Purification and quantification of CBM3-ZZ

The CBM3-ZZ protein was purified by affinity chromatography using an IgG Sepharose 6 Fast Flow column (GE Healthcare) in an ÄKTA 10 Purifier system. The column was equilibrated with 5 column volumes of TST buffer and then loaded with 2 mL of the supernatant containing CBM3-ZZ, unbound proteins were washed away in a single step with 10 column volumes of TST. The bound CBM3-ZZ was eluted with 0.5 M acetic acid, pH 2.8. The pH of the collected fractions of CBM3-ZZ was immediately neutralized with 3.2 M Tris buffer, pH 10.96.

The purity of CBM3-ZZ fusion protein was determined by sodium dodecyl sulfate polyacrylamide gel electrophoresis (SDS-PAGE) in a 12% acrylamide gel. All samples were diluted prior to denaturation in reducing conditions with 5 µL of 1 M dithiothreitol at 100 ºC for 5 minutes. Gels were stained with

Coomassie Brilliant Blue. A 10-250 kDa protein ladder (Bio-Rad) was used as a molecular mass marker. Images of SDS-PAGE gels were obtained with a GS-800™ Calibrated Densitometer (Bio-Rad). The purified CBM3-ZZ concentration was determined by the BCA (Bicinchoninic Acid) Protein Assay using the Pierce® BCA Protein Assay kit (microplate procedure), according to the manufacturer's instructions. A buffer composed of 10 mM NaHEPES, pH 7.5, 2 mM imidazole, 200 mM NaCl and 1 mM $CaCl_2$ was used as diluent. The purified CBM3-ZZ was stored at -20 ºC before use.

3.6 Spots assays

The device fabrication using the wax patterning method was performed as described in section 3.5. Throughout this work, the patterned spots on paper used were 4 mm diameter circles with 0.4 mm line thickness. (Figure 3-2).

Figure 3-2 Design of the 4 mm diameter PAD used for the spot assays. The thickness of the printed wax lines in both structures is 0.4 mm. After melting and diffusion of the wax, the width of the wax barriers increases to 1 mm.

3.6.1 Immobilization of the CBM3-ZZ:antibiotin IgG conjugate in paper

In all the performed assays, 2 µL of the complex CBM-ZZ:antibiotin IgG (ratio1:2.5) was applied on the patterned spots in fractions of 0.5 µL, letting it air dry at room temperature between applications. The mixture of 2 pmol of CBM3-ZZ and 5 pmol of antibiotin IgG in TST was pre-incubated for 30 minutes at room temperature before being spotted on paper.

3.6.2 Capture of biotin-AuNPs by antibodies immobilized on paper via CBM3-ZZ vs physical adsorption

The capture of biotin labeled gold nanoparticles was evaluated by applying different amounts of biotin-AuNPs on spots patterned on paper (0, 0.6, 1.2 and 2.3 fmol) that contained either the CBM3-ZZ:antibiotin IgG complex or physically adsorbed antibiotin IgG. As a control, biotin-AuNPs were applied to a plain spot. The mixture of the CBM3-ZZ:antibiotin IgG conjugate and its consequent immobilization in paper patterned spots was performed as explained previously (section 3.6.1). The physical adsorption was performed using the same steps of the immobilization of the CBM3-ZZ:antibiotin IgG complex. A total volume 2 µL of TST buffer with 5 pmol of antibiotin was prepared and applied on paper in fractions of 0.5 µL, letting it air dry at room temperature between applications. After the immobilization is done and the paper is dry, 2 µL of TST containing the amounts of biotin-AuNPs specified above are applied in the quantity previously referred were added. After drying at room temperature, results were recorded by scanning the patterned spots with a HP scanjet 4400c scanner, with settings set to a medium level

of distinctness and a dpi of 600 (Figure 3-3A). The analysis of the spots was made by measuring the mean grey intensity using the image processing program ImageJ (NIH, National Institutes of Health). The method used was described by Jokerst et al. [62]. Using this software, the original image is first converted to an 8-bit grey scale image (Figure 3-3B), which is then inverted (Figure 3-3C), so that the grey intensity measured increases with the decreasing grey color developed. Then the reaction zone is selected and the mean grey intensity is measured. The mean grey intensity was calculated by discounting the mean grey intensity of the background. A spectrophotometric analysis was done of the three different mixtures: i) 2.3 fmol biotin-AuNP in 30 µL of TST; ii) 5 pmol of antibiotin IgG and 2.3 fmol of biotin-AuNP in 30 µL of TST; iii) CBM3-ZZ;antibiotin IgG (2 pmol:5 pmol) in 30 µL of TST. These mixtures were added in a 384-well microplate and read in a SPECTROstar Nano (BMG Labtech).

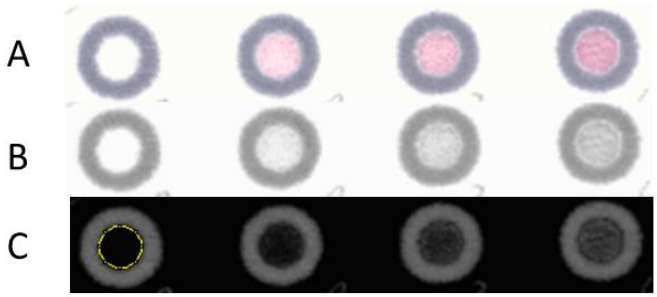

Figure 3-3 Protocol used for the analysis of the spots using ImageJ software. **A)** Image obtained by scanning the paper spots used in the capture of biotin-AuNPs by the CBM3-ZZ:antibiotin IgG conjugate. **B)** Image in A is converted to 8-bit grey scale. **C)** Image in B is inverted, so that a negative image is produced and the area corresponding to the reaction zone is selected (yellow circumference).

3.6.3 Capture of biotin-AuNPs by antibodies immobilized on paper via CBM3-ZZ vs control conditions

To perform this assay, spots in three different conditions were prepared. A spot was functionalized by physical adsorption of 5 pmol of antibodies per spot, another spot was given a function by biochemical immobilization of 2 pmol of CBM3-ZZ and 5 pmol of antibodies, and a last spot was prepared with no function. In the capture test, an antibiotin IgG was used while in the negative controls an anti-FITC IgG was used. To all the spots 2.3 fmol of biotin-AuNP in 2 µL of TST were applied. All the preparation of the mixtures and immobilization steps were made in the same conditions previously described. After drying at room temperature, the results were recorded using HP Scanjet 4400c scanner and processed by ImageJ software, by measuring the mean grey intensity after converting the acquired images to 8-bit grey scale and inverting the colors.

3.6.4 Optimization of AuNPs applied on paper

The procedure used to apply sample solutions on the patterned spots on paper was studied by applying a total of 2 µL of a solution containing 2.3 fmol of biotin-AuNPs in TST buffer to spots

functionalized as described before. One spot without anything applied on its surface, one functionalized by physical adsorption of 5 pmol of antibiotin IgG, and one spot functionalized by the conjugate CBM3-ZZ:antibiotin IgG prepared as previously described. The 2 µL solution of AuNPs was applied on each of the different spots as 4 x 0.5 µL, 2 x 1 µL or 1 x 2 µL. After drying at room temperature, the results were recorded using HP Scanjet 4400c scanner and processed by ImageJ software.

3.6.5 Scanning Electron Microscopy (SEM)

Observation of the spots in different conditions was done by scanning electron microscopy (SEM) using a FEG-SEM JEOL JSM7001F equipment. Prior to analysis, samples were coated with a chromium layer using a Polaron E5100 coating system (Quorum Technologies). The samples analyzed were the 3 different conditions evaluated before, one spot with only the Biotin-AuNPs, one spot with antibiotin IgG physical adsorbed and Biotin-AuNPs, and one spot with the CBM3-ZZ:antibiotin IgG conjugate immobilized and Biotin-AuNPs. In all the mentioned conditions, 2.3 fmol of Biotin-AuNP in 2 µL of TST buffer was used.

3.6.6 Spot assays performance

The ability of the bioactive paper to detect different amounts of biotinylated AuNPs was studied as a proof of concept for the use of gold nanoparticles as a colorimetric detection method in immunoassays. For this, the spots were prepared by immobilizing CBM3-ZZ:antibiotin IgG following the method previously explained. Solutions with different quantities of gold nanoparticles (0, 0.6, 1.2, 2.3, 4.6, 9.2 and 18.5 fmol) in TST were prepared and applied on the spots previously functionalized. After drying at room temperature, the results were recorded using a HP Scanjet 4400c scanner and processed by ImageJ software, by measuring the mean grey intensity after converting the acquired images to 8-bit grey scale and inverting the colors.

3.6.7 Rehydration of AuNPs spoted on paper

To study the possibility of rehydration of gold nanoparticles previously deposited on the spots, 2 µL of solution containing 2.3 fmol of biotin-AuNPs was applied in each spot. After air drying at room temperature, the spots were scanned using a HP Scanjet 4400c scanner. The rehydration of the previously spotted biotin-AuNPs was done using two different conditions. One using 5 pmol of antibiotin IgG in 2 µL TST, and another with 2 µL of the pre-incubated CBM3-ZZ:antibiotin IgG conjugate prepared as described beforehand. The rehydration step was done by applying the 2 µL solutions at once in each spot. The spots were washed two times with 2 µL TST. After drying the spots were recorded using HP Scanjet 4400c scanner, and the images acquired before and after the rehydration step were analyzed using the ImageJ.

3.7 Microfluidic Channels Assays

µPADs with microchannels of 2.4 mm nominal width and 28 mm nominal length plus a reservoir of 13 mm nominal length were defined by wax-printing lines with 0.4 mm of thickness according to the design shown in Figure 3-4.

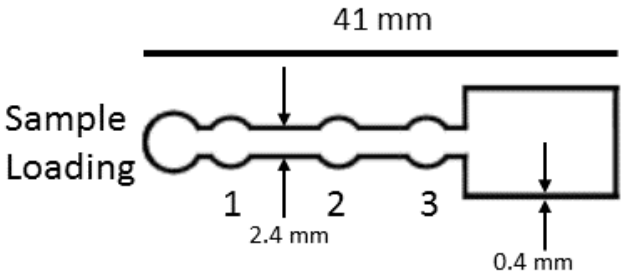

Figure 3-4 Design of the µPADs used. The spots are numbered for better identification throughout this thesis. The thickness of the printed wax lines in both structures is 0.4 mm. After melting and diffusion of the wax, the width of the wax barriers increases to 1 mm.

3.7.1 Capture of biotin-AuNPs by immobilized antibodies via CBM3-ZZ inside wax-printed channels on paper versus physical adsorption

µPADs were prepared by applying 2 µL of a solution containing 5 pmol of antibiotin IgG or 2 µL mixtures of 2 pmol of CBM3-ZZ and 5 pmol of antibiotin IgG in the detection zone (spot 2/T). Solutions were always pre-incubated at room temperature for 30 min. The dispensing of the 2 µL solutions was done in fractions of 0.5 µL to assure that the antibiotin IgG and the CBM3-ZZ:antibiotin IgG conjugates remained mostly in the center of the detection zone, without flowing by capillarity through the channel. After drying, different quantities of Biotin-AuNPs (0.6, 1.2, 2.3, 4.6 fmol) diluted in 15 µL of TST were applied in the sample loading zone with the microfluidic device hanging in the air (Figure 3-5). Each µPAD was then washed by adding 15 µL of TST to the sample loading zone. Once dried, µPADs were scanned using a HP Scanjet 4400c scanner. The mean grey intensity of the capture spots was then measured with the ImageJ software as previously described. The mean grey intensity takes the background signal into consideration.

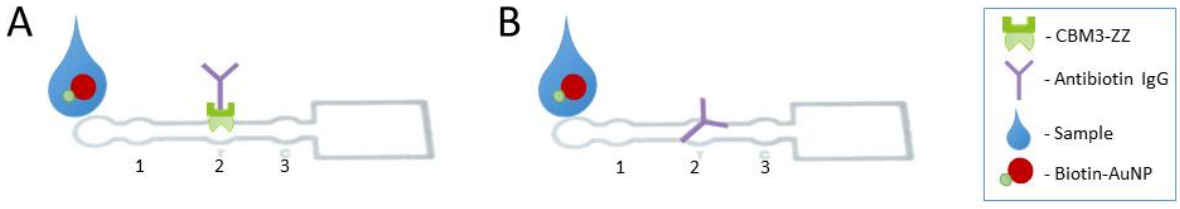

Figure 3-5 Schematic of the assay for the capture of biotinylated gold nanoparticles. **A)** Immobilization of antibiotin IgG (5 pmol) through biochemical coupling with CBM3-ZZ (2 pmol) in reaction zone 2. **B)** Immobilization of antibiotin IgG (5 pmol) by physical adsorption in reaction zone 2.

3.7.2 Conjugation studies

The ability to separately deposit the different reagents on the μPAD, leading to a detectable signal in the capture zone, with the addition of a buffer to the sample loading zone, was tested by depositing 2.3 fmol of biotin-AuNPs in spot 1, 5 pmol of antibiotin IgG in spot 2 and 2 pmol of CBM3-ZZ in spot 3. As a control, and instead of using antibiotin IgG, FITC-Human IgG was applied. Once all spots were dry, 15 μL of TST were loaded into the sample loading zone and allowed to flow by capillarity with the device hanging in the air (Figure 3-6A). The same procedure was done without pre-depositing the Biotin-AuNPs, and instead loading the 2.3 fmol of biotin-AuNPs in 15 μL of TST to the sample loading zone (Figure 3-6B). All the μPADs were washed with 15 μL of TST. After drying at room temperature the results were recorded using a HP Scanjet 4400c scanner. The fluorescence was analyzed by a Leica DMLB fluorescence microscope (Leica Microsystems, Wetzlar, Germany) coupled with an Olympus E-PM1 photographic camera.

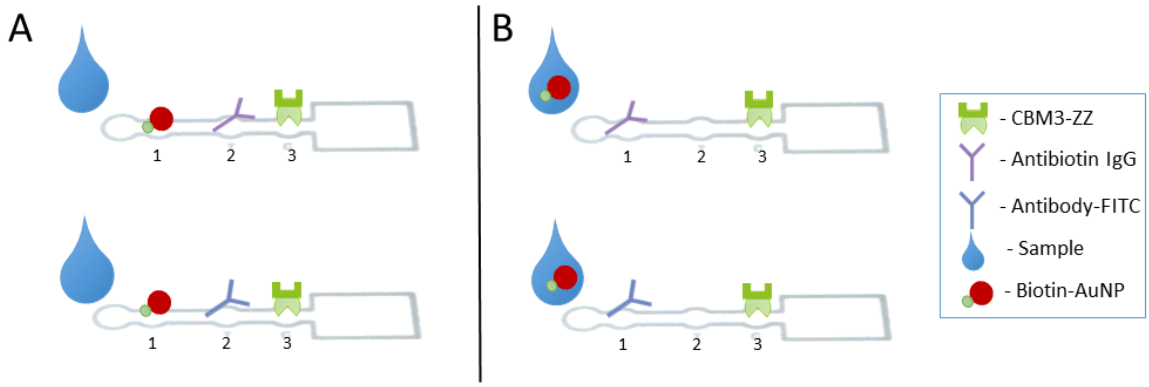

Figure 3-6 Schematic of the assays designed to study the conjugation of the different pre-deposited components. In the top μPADs, antibiotin IgG is used, while in the bottom μPADs an IgG antibody labeled with FITC was used**. A)** Assays with the biotin-AuNPs pre-deposited in the paper. **B)** Assays with the biotin-AuNPs in the sample.

To further study the ability of the conjugate CBM3-ZZ:antibitotin IgG to be formed in the μPAD during the flow of the sample by capillarity was done by immobilizing 2 pmol of CBM3-ZZ in both spot 2 and spot 3, and either 5 or 10 pmol of antibiotin IgG in spot 1. The μPADs were then loaded with 4.62 fmol of Biotin-AuNPs in 15 μL of TST buffer in the sample loading zone (Figure 3-7B). To compare the signal achieved through this method, several μPAD were prepared by applying the CBM3-ZZ:antibiotin IgG, formulated and pre-incubated as previously described, in both spot 2 and spot 3 of the μPADs and loading the channel with various quantities of biotin-AuNPs (2.9, 3.5, 4.0 and 4.6 fmol) in 15 μL of TST buffer (Figure 3-7A). The μPADs were washed with additional 15 μL of TST. Once completely dry, all the μPADs were scanned using a HP Scanjet 4400c scanner and analyzed using ImageJ software.

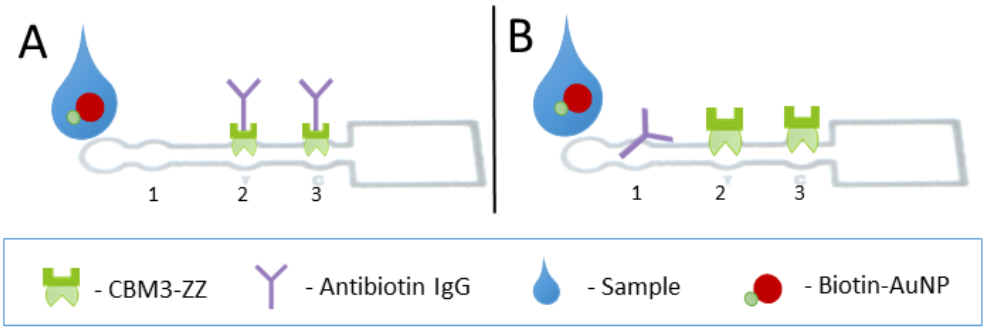

Figure 3-7 Schematic of the assays designed to study the conjugation of the antibody pre-deposited on paper. **A)** The CBM3-ZZ:antibiotin IgG conjugate was pre-incubated at room temperature prior to the immobilization. **B**) The antibodies and the CBM3-ZZ were separately deposited in the µPAD. Two different quantities of physically adsorbed antibody were tested: 5 and 10 pmol.

3.7.3 Use of Plastic Adhesives

The effect of isolating the µPADs with an adhesive tape ARcare® 93241 (Adhesives Research Ireland Ltd, Limerick, Ireland) was studied. This tape is made of clear polyester film and an acrylic medical grade adhesive. All assays were done using three different conditions: i) a control without adhesive tape (Figure 3-8A); ii) a µPADs isolated underneath with the adhesive tape (Figure 3-8B); iii) a µPADs isolated underneath and above, leaving only the sample loading zone uncovered (Figure 3-8C). In a first instance, the capillary migration under the different conditions was studied by applying a 15 µL volume of an orange dye and recording with an Olympus E-PM1 camera. Next, a simple capture assay, as described in section 3.7.1, was performed by first immobilizing the CBM3-ZZ:antibiotin IgG conjugate in spot 2 of the microfluidic device, which once dry was isolated with adhesive tape as outlined in Figure 3.8.

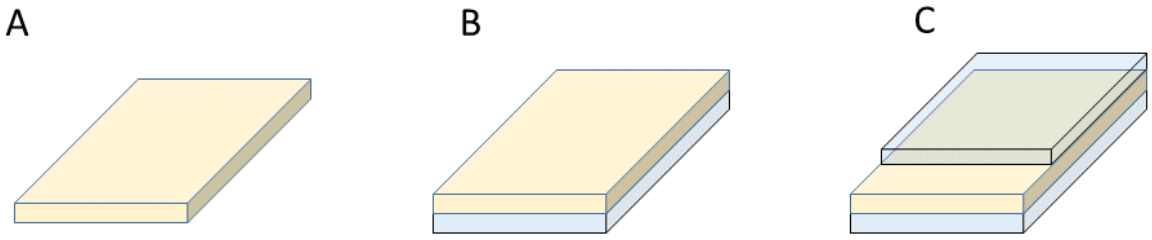

Figure 3-8 Scheme of the conditions used with adhesive tape to isolate the µPADs. **A)** Control µPAD. **B)** µPAD isolated underneath with adhesive tape. **C)** µPAD isolated with adhesive tape both underneath and above leaving the sample loading zone uncovered.

Chapter 4. Results and Discussion

4.1 Spot assays

4.1.1 Capture of biotin-AuNPs by antibodies immobilized on paper via CBM3-ZZ vs physical adsorption

One of the objectives of this work was to evaluate, through proof-of-concept experiments, whether the fusion protein CBM3-ZZ could be used in the context of antigen detection in PADs. In a first instance, several spots were fabricated on paper by wax printing, outlining 4 mm circular reaction areas by hydrophobic barriers. Different immobilization strategies were used to functionalize the fabricated spots with antibodies, a biochemical coupling with a CBM3-ZZ fusion versus a physical adsorption approach. In the first case, CBM3-ZZ fusions (2 pmol/spot) and antibiotin IgG (5 pmol/ spot) were pre-incubated before spotting, while in the physical adsorption strategy antibiotin IgG (5 pmol/spot) was spotted directly on paper. The ratio of CBM3-ZZ:antibody IgG was determined in previous work of Rosa *et al.* [24]. Different quantities of biotin labeled gold nanoparticles (biotin-AuNPs) were then applied to those spots. Spots where only biotin-AuNPs were added were used as controls (Figure 4-1).

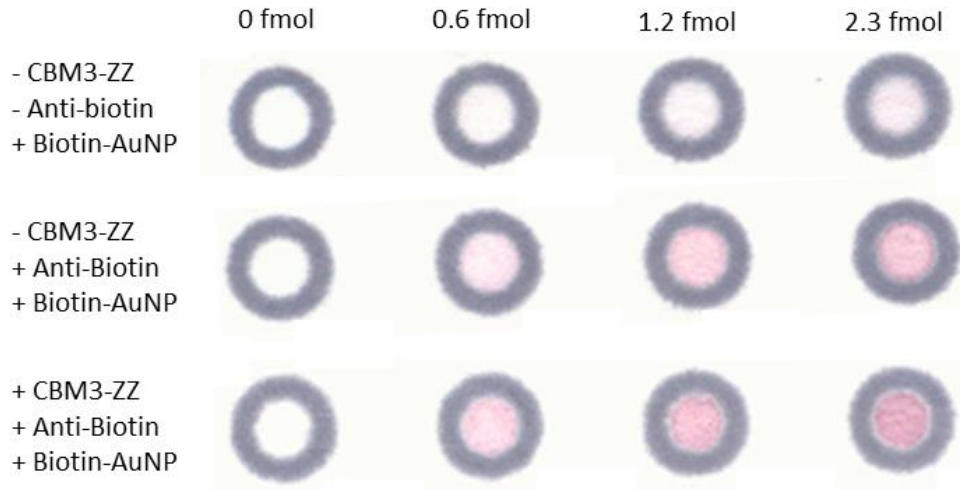

Figure 4-1 Capture of biotin-AuNPs by antibiotin IgG immobilized in paper spots. The first row shows control experiments were different amounts of biotin-AuNPs (0- 2.3 fmol) were applied to non-functionalized spots. In the second row, biotin-AuNPs were captured by physically adsorbed antibiotin IgG (5 pmol/spot). In the third row, the biochemical coupling of CBM3-ZZ (2 pmol/spot) and antibiotin IgG (5 pmol/spot) was evaluated. The 4 mm circular areas were defined on paper by wax-printing.

Analyzing the spots in Figure 4-1, it is noticeable the virtually absence of color in the spots where only the biotin-AuNPs were applied, while in the spots where either of the antibodies immobilization strategies were used, there is an increasing intensity of red color with the increase of biotin-AuNPs applied. To further analyze the results, the mean grey intensity of each of the spots was measured using ImageJ software (Figure 4-2).

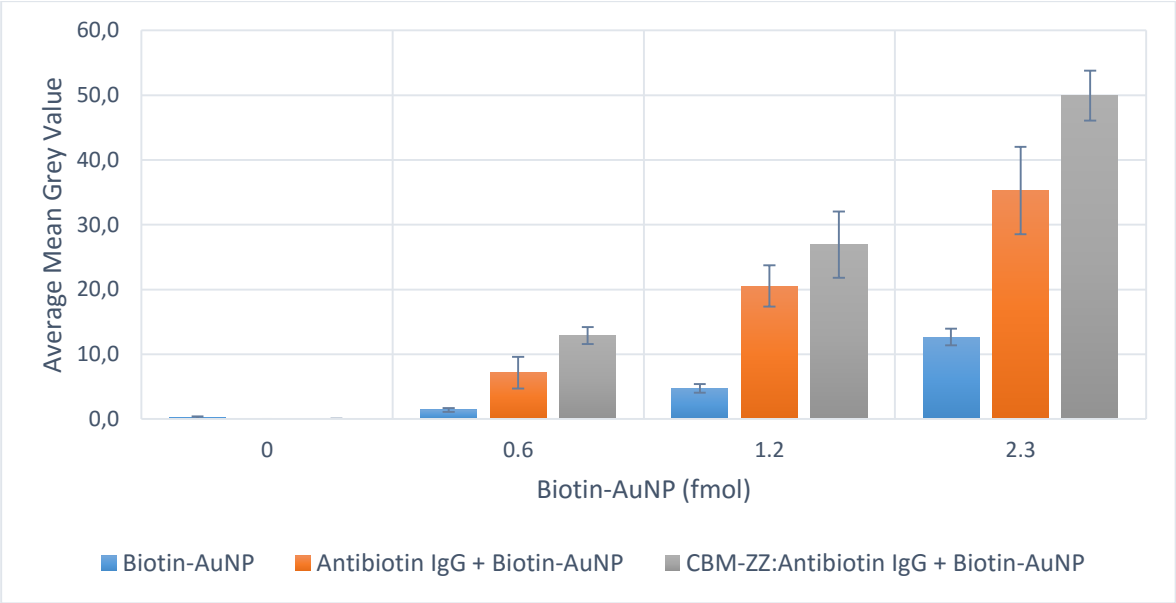

Figure 4-2 Capture of biotin-AuNPs by antibiotin IgG immobilized in paper spots. The figure shows a comparison of the average mean grey intensity of the spots prepared with the different immobilization strategies represented in Figure 4-1. Each one of the represented test conditions was done in triplicate and the error bars represent the standard deviation.

The higher color intensity of the spots where the biochemical coupling of the antibiotin IgG by CBM3-ZZ was used as an immobilization strategy is observable by analyzing figures 4-1 and 4-2. The physical adsorption of the antibody also display a higher intensity of the color developed when compared with the simple deposition of biotin-AuNPs on paper, but inferior to the spots with CBM3-ZZ:antibiotin IgG conjugate. This weaker signal is probably due to the random orientation of antibiotin IgG on the surface of the paper, which can lead to a reduced recognition and ability to capture the biotin-AuNPs due to the steric hindrance of binding sites [4], [8], [24]. The physical adsorption of antibodies to the paper surface is established mainly by weak interactions, such as Van der Walls and electrostatic forces [8], and as such if a washing step, of the strips of paper with the spots, was done between the immobilization step and the addition of the sample, a portion of the physically adsorbed antibodies would be removed from the spots [24]. Even though the filter paper may still have a capacity to adsorb a great quantity of antibodies the signal measured would be lower, while the color intensity of the spots where biochemical immobilization was applied would be constant.

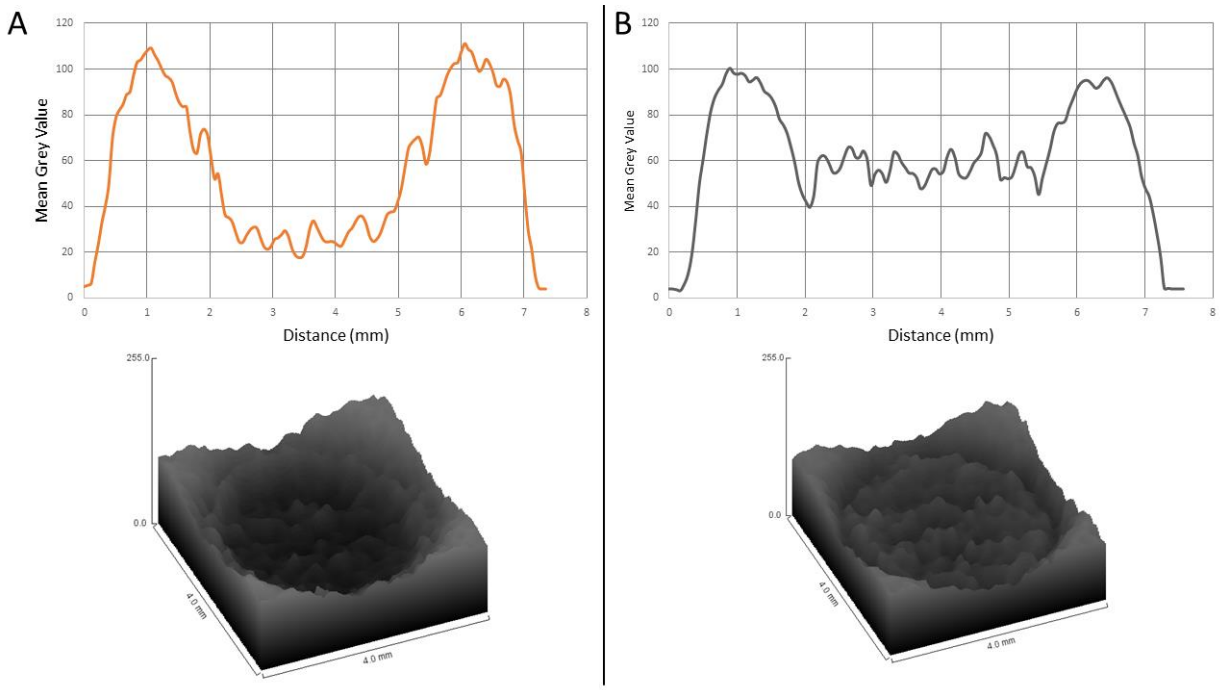

Figure 4-3 Plot profile (upper graph) and surface plot of spots where Biotin-AuNPs were captured by antibiotin antibodies immobilized by adsorption or biochemical coupling**. A)** Physical adsorption of antibiotin IgG (5 pmol/spot) and 2.3 fmol of biotin-AuNPs**. B)** Immobilization through biochemical coupling of CBM3-ZZ (2 pmol/spot) and antibiotin IgG (5 pmol/spot) pre-incubated and addition of a sample with 2.31 fmol of biotin-AuNP.

Figure 4-3 data concern the two bottom spots of the last column of figure 4-1 where the two different approaches to immobilization are shown. The plot profile analysis was done in ImageJ by drawing a line through the middle of the spot, and the surface plot was acquired by delineating a circular area covering the whole spot and using the surface plot tool. In the plot profile graphs, the maxima of the curves correspond to the wax barriers limiting the reaction area. Analyzing the spot with physically adsorbed antibodies (Figure 4-3A) it is possible to notice that there is an accumulation of color near the walls of the spot, at around 2.0 mm and 5.2 mm. This phenomenon is called the coffee ring effect, and it occurs because a drop of a liquid tends to spread by capillarity flow from the center to the edges, bringing the particles suspended in the solution to the walls of the spot [63]. After subsequent evaporation, the concentration of the particles will be higher on the edges than in the center. In the case of biochemical immobilization, this effect is not observable, being the intensity of the color evenly distributed through the spot, although not being completely homogeneous (Figure 4-3B). CBMs are molecules with high affinity to cellulose and spontaneously bind to it. As such when the CBM3-ZZ:antibiotin IgG conjugate is immobilized in paper and the sample with biotin-AuNPs is applied, the antibiotin IgG will readily capture the biotin-AuNPs, which will not be able to flow to the edges.

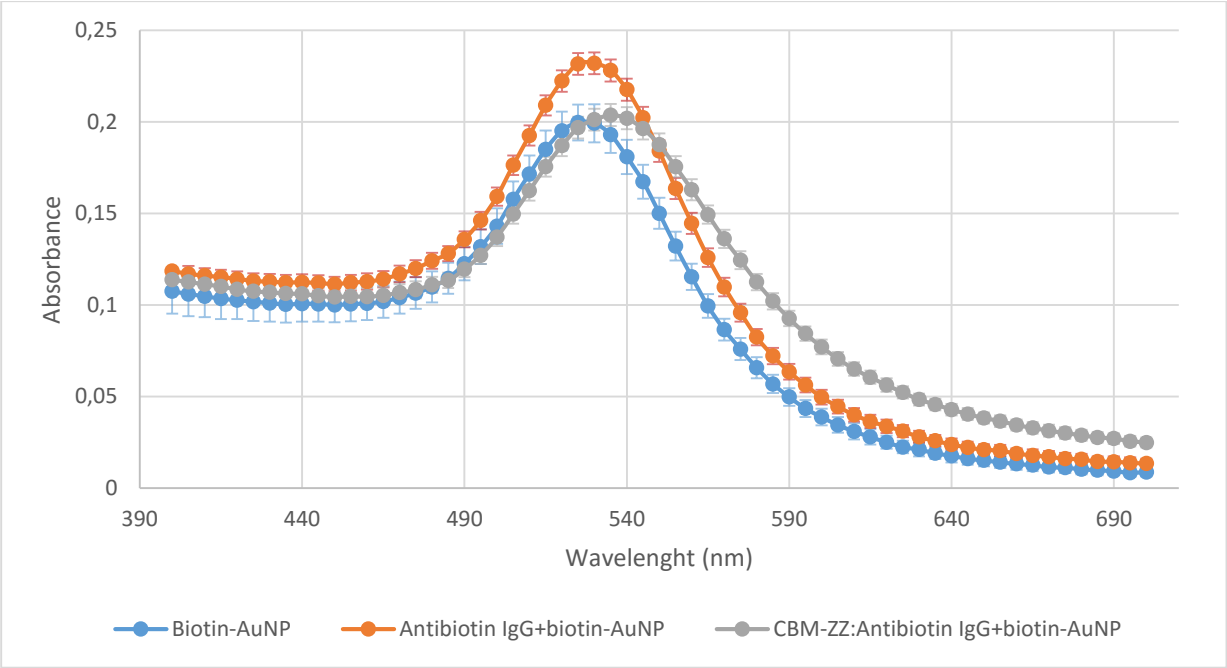

Figure 4-4 UV/visible spectra of biotin-AuNPs in different conditions.

In figure 4-4, the UV/visible spectra of the different mixtures used in the immobilization strategies are represented. The spectra of the biotin-AuNPs and of the antibiotin IgG+biotin-AuNPs mixture displays the normal behavior of 40 nm gold nanoparticles with a peak of absorbance between 525 and 530 nm [33], [34], [64]. As for the spectrum of the mixture of CBM3-ZZ:antibiotin IgG and biotin-AuNPs, and apart from small shift in the peak of absorbance to 535 nm, no significant differences are detectable.

4.1.2 Capture of biotin-AuNPs by antibodies immobilized on paper via CBM3-ZZ vs control conditions

To investigate whether the increase in the intensity of the colors generated in the spots was due to the recognition of the biotin-AuNPs by the antibiotin IgG, a control assay was designed where an anti-FITC IgG was used instead of antibiotin IgG. To test this, the same conditions were used for the immobilization methodologies. The physical immobilization was done by applying 5 pmol of either antibiotin IgG or anti-FITC IgG per spot. The biochemical immobilization was performed by dispensing a pre-incubated mixture of 2 pmol of CBM3-ZZ and 5 pmol of either of the referred antibodies. Plain paper spots were used as a control.

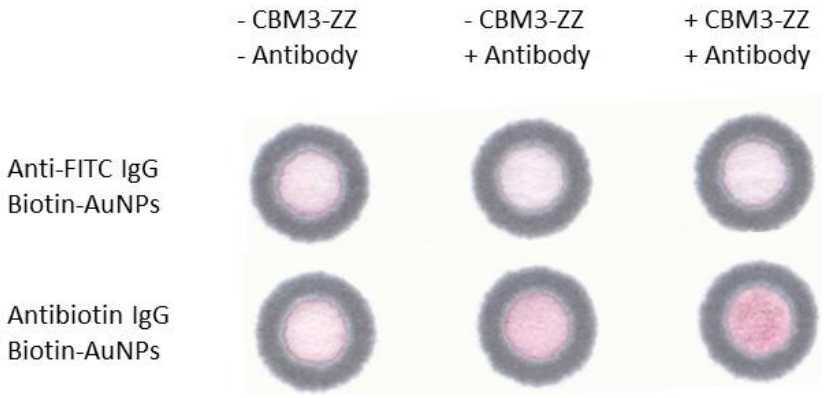

Figure 4-5 Capture of biotin-AuNPs by antibiotin IgG using different immobilization strategies versus a control assay using an anti-FITC IgG. Negative controls with anti-FITC IgG are shown in the top row, and assays with antibiotin IgG are shown in the bottom row. On the left column are the biotin-AuNPs applied on paper, the middle column refers to the physical adsorption assays and the last column are the biochemical coupling assays. 2.3 fmol of biotin-AuNPs were applied to each spot.

Analyzing the spots of figure 4-5 by naked eye, it is possible to notice a higher intensity of the color in the spot corresponding to the biochemical immobilization of the CBM3-ZZ:antbiotin IgG conjugate when compared to all the other spots, corroborating the data previously acquired. The spots where the antibody used was an anti-FITC IgG show no variation in the intensity of the color.

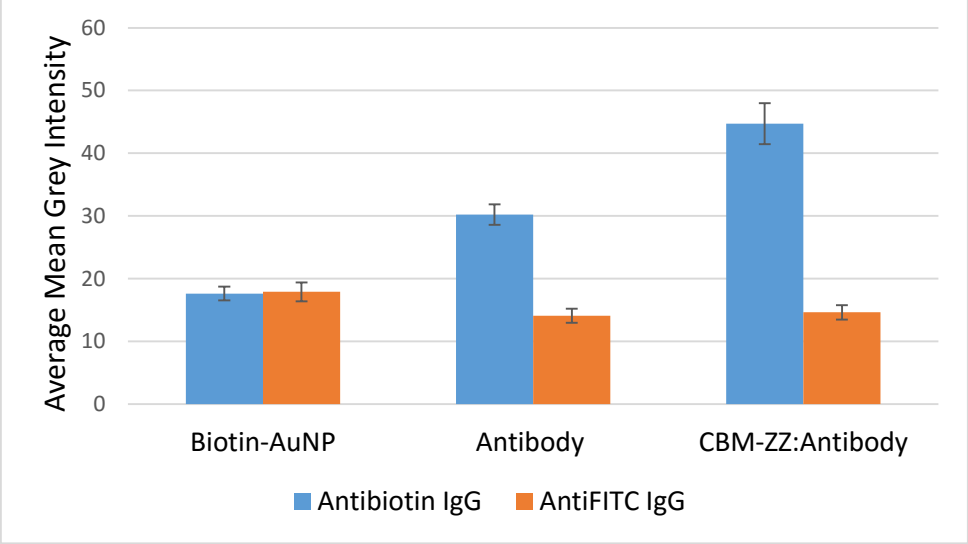

Figure 4-6 Capture of biotin labeled gold nanoparticles by antibiotin IgG using different immobilization strategies versus a control assay using an anti-FITC IgG. The assay was performed in triplicates and the error bars represent the standard deviation.

Figure 4-6 shows the analysis of the intensity of the color developed in the paper spots. The negative control, using anti-FITC IgG, did not show a significant variation, even though the average mean grey intensity was slightly higher in the spot with no immobilization strategy applied. Significant increases in color were detected when physically or biochemically immobilizing antibiotin IgG. The development of a more intense red color in the spots with the biochemically-coupled antibiotin IgG can

be attributed to a more correct orientation of the antibody provided by the CBM3-ZZ fusion and hence to a more efficient recognition of the antigen.

4.1.3 Optimization of AuNPs applied on paper

To study the way the sample addition affect the final color developed in each immobilization condition, an assay where the sample solution with AuNPs was is added in fractions of the total volume was designed. In spots non-functionalized, and functionalized by either physical adsorption or biochemical coupling as previously described, a total volume of 2 µL of solution containing 2.3 fmol of biotin-AuNPs in TST was applied in fractions of 0.5, 1 or 2 µL.

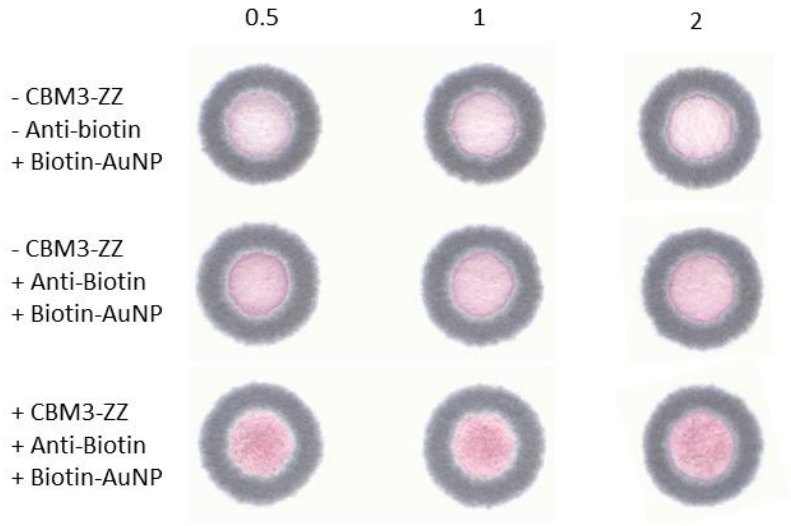

Figure 4-7 Evaluation of the intensity of the color obtained in the different immobilization approaches in study when the sample is applied in different volume. Each column concerns the fraction of volume (in µL) which was applied in each spot, always totaling 2 µL applied per paper spot. The top row concerns the spots with only the biotin-AuNPs applied. The middle row regards the physical immobilization of antibiotin IgG. The bottom row concerns the biochemical coupling of the antibiotin IgG by CBM3-ZZ.

Analyzing figure 4-7, it is noticeable the same pattern between the different immobilization techniques in study. While the spots where the physical adsorption of antibiotin IgG was used and the spots where only the biotin-AuNP were applied display the coffee ring effect, which is noticeable by the accumulation of the gold nanoparticles near the edges of the reaction zone, the biochemical coupling of the CBM3-ZZ:antibiotin IgG results in a more uniform and concentrated signal.

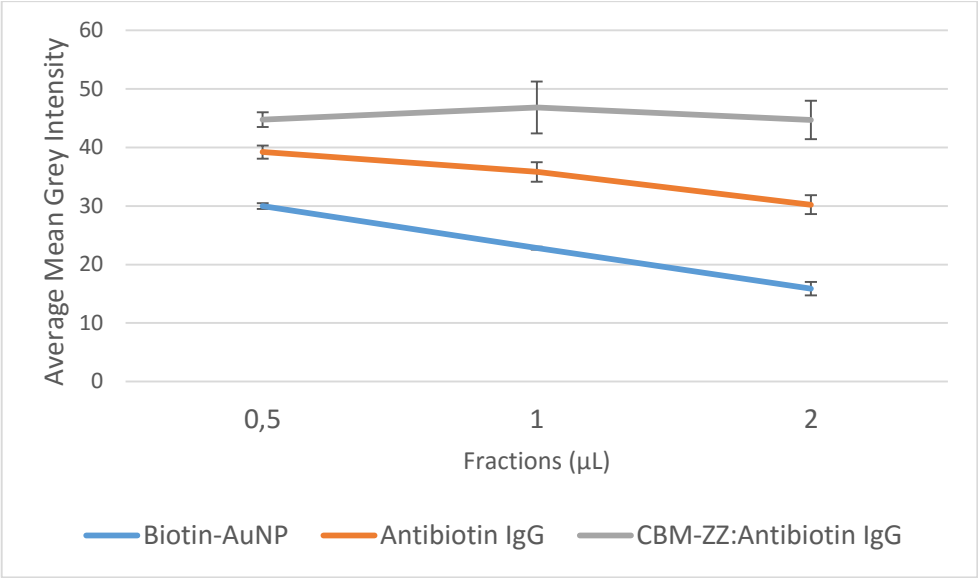

Figure 4-8 Evaluation of the intensity of the color obtained in the different immobilization approaches in study when the sample is applied in fractions of the total volume. The assay was performed in triplicates and the error bars represent the standard deviation.

Figure 4-8 show the average mean grey intensity as a function of the volume of fractions applied of the spots in figure 4-7. The intensity of the color in the spots with the CBM3-ZZ:antibiotin IgG conjugate immobilized display a color without a significant variation in its intensity, while both the physical adsorption approach and the spots with only the biotin-AuNP applied on paper show a decreasing intensity of the color with the increase of the volume applied with the sample. This phenomenon is, once more, related to the coffee ring effect [63]. As the molecules in these spots are not strongly bound to the paper, when a single addition of 2 µL is used the molecules in suspension tend to be pushed to the edges. Although the addition of the samples in four fractions of 0.5 µL is enough to wet all the reaction zone of the spot, the volume of buffer is not enough to make the molecules in suspension get dragged towards the edges of the spots, thus being more deposited near the center of the spots and giving a higher intensity when analyzed by ImageJ.

4.1.4 Scanning Electron Microscopy (SEM)

Spots containing biotin-AuNPs captured by physically or biochemically immobilized antibiotin IgG were analyzed by SEM (Figure 4-9).

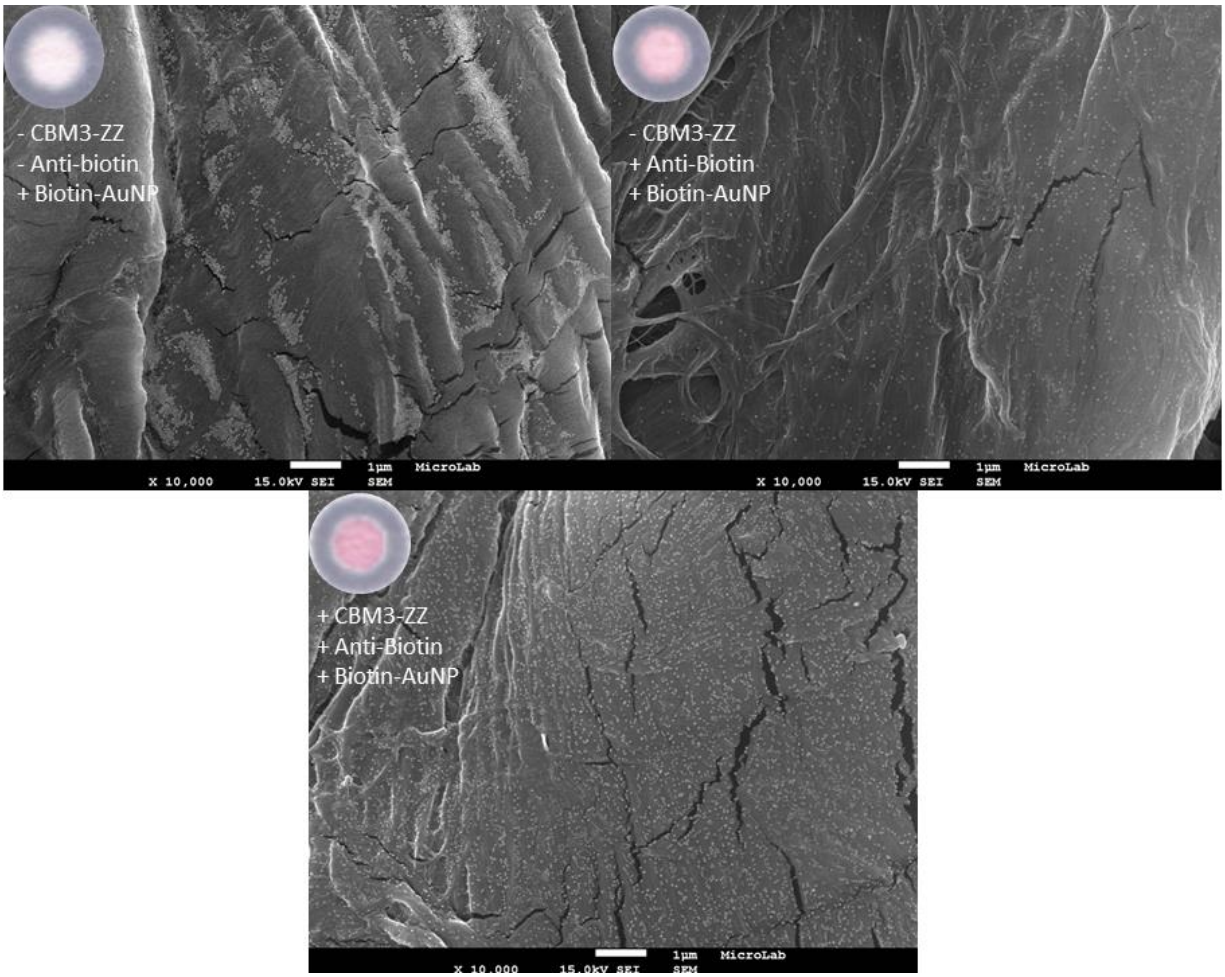

Figure 4-9 SEM images of spots containing biotin-AuNPs captured by physically or biochemically immobilized antibiotin IgG. The upper left image corresponds to a control spot with only biotin-AuNPs applied on paper. The upper right image concerns a spot where biotin-AuNPs were captured by physically adsorbed antibiotin IgG. The bottom image corresponds to a spot where biotin-AuNPs were captured by a biochemically immobilized CBM3-ZZ:antibiotin IgG conjugate. All images were acquired at a 10,000x magnification. The scale of each photograph is defined by the horizontal white bar which corresponds to 1 µm.

The SEM image of the control spot with only the biotin-AuNPs shows that the gold nanoparticles accumulate together in the grooves created by the cellulose fibers (Figure 4.9, top left). On the contrary, in the SEM image of the spot prepared by biochemical immobilization of antibiotin-IgG with the CBM3-ZZ fusion, a uniform distribution of the gold nanoparticles throughout the whole observable surface of the paper is visible (Figure 4.9, bottom). The image obtained from a spot where the physical immobilization of the antibiotin IgG was used, show a in between state of the other conditions (Figure 4.9, top right). In this condition the gold nanoparticles are not accumulated as in the first case, but they also are not so evenly distributed as in the biochemical coupling. This is due to two main reasons: the random orientation of antibiotin IgG on the surface of the paper, which can lead to a reduced recognition and ability to capture the biotinylated gold nanoparticles [4], [8], [24]; the physical adsorption of antibodies to the paper surface is established mainly by weak interactions, and as such, these can be washed to the edges of the spot [8].

The difference in the developed color between the spots with only the biotin-AuNPs and the spots where the nanoparticles were captured by the CBM3-ZZ:antibiotin IgG conjugate may be due to two factors: i) as the CBM3-ZZ has affinity for cellulose and will orientate the antibiotin IgG correctly, the biotin labeled gold nanoparticles will be forced to stay at the surface of the paper, while without any biosensor immobilization for recognition of the gold nanoparticles those will flow through the paper fibers and can become hidden between the fibers translating in a low intensity color observed; ii) the optical properties of gold nanoparticles change when there is an aggregation of the particles leading to the conduction electrons near each particle surface to become delocalized and shared amongst neighboring particles. Consequently, the surface plasmon resonance shifts to lower energies, causing the absorption and scattering peaks to shift to longer wavelengths. UV/Visible spectroscopy can be used as a simple and reliable method for monitoring the stability of nanoparticle solutions. As the particles destabilize, the original extinction peak will decrease in intensity, due to the depletion of stable nanoparticles, and often the peak will broaden or a secondary peak will form at longer wavelengths, due to the formation of aggregates [34], [36], [64], [65]. This phenomenon which happens in solution is probably occurring in the paper spots in this study.

Additional images were obtained through SEM but using a different detector, a Back-scattered Electron Detector (BSE) (Figure 4.10). In simple terms, this detector will stress the difference between the atomic species present based on their mean atomic number (Z). Thus, a "brighter" BSE intensity correlates with greater average Z in the sample, and "darker" areas have lower average Z [66].

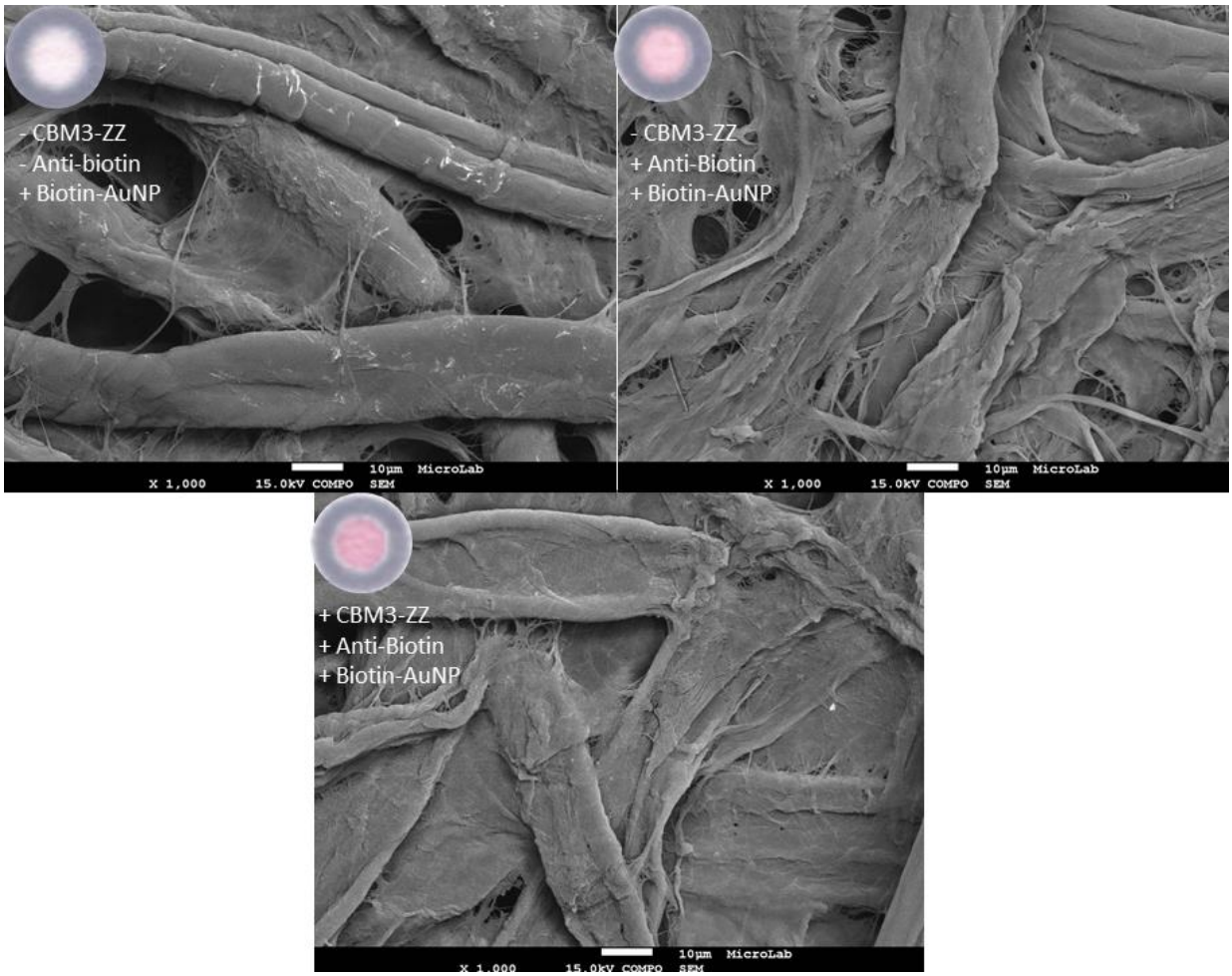

Figure 4-10 SEM images of spots containing biotin-AuNPs captured by physically or biochemically immobilized antibiotin IgG obtained with a BSE detector. Upper left image concerns a spot with only biotin-AuNP applied on paper. The upper left image corresponds to a control spot with only biotin-AuNP applied on paper. The upper right image concerns a spot where biotin-AuNPs were captured by physically adsorbed antibiotin IgG. The bottom image corresponds to a spot where biotin-AuNPs were captured by a biochemically immobilized CBM3-ZZ:antibiotin IgG conjugate. All images were acquired at a 1,000x magnification. The scale of each photograph is defined by the horizontal white bar which corresponds to 10 µm.

As gold has a higher atomic number, the biotin-AuNPs will appear brighter in the images in contrast to the cellulose fibers. In the spots with only the biotin-AuNP, the accumulation of the gold nanoparticles together is clearly noticeable (Figure 4.10, top left), while in spots with the immobilization of antibiotin IgG (Figure 4.10, top right and bottom), the nanoparticles are more evenly distributed, as seen before.

4.1.5 Spot assay performance

The ability of the bioactive paper to detect a broader range of amounts of biotin-AuNPs was studied in wax printed 4 mm spots with CBM-ZZ:antibiotin IgG conjugate (2 pmol:5 pmol) immobilized and quantities of biotin-AuNPs between 0 and 18.5 fmol in TST.

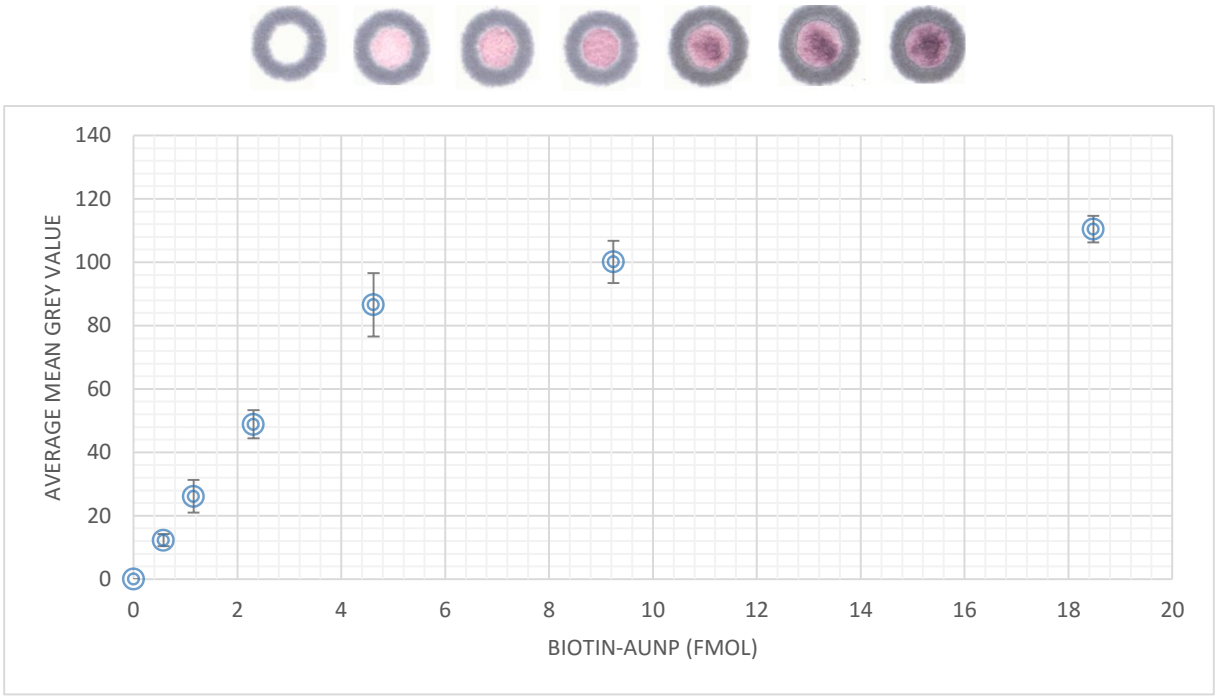

Figure 4-11 Capture of biotin-AuNPs by CBM3-ZZ:antibiotin IgG conjugate (2 pmol:5 pmol) immobilized on 4 mm spots on paper. Quantities of biotin-AuNPs were between 0 and 18.5 fmol. The assay was performed in triplicate and the error bars represent the standard deviation.

Analyzing the spots it is possible to notice the development of a darker color in the center region of the spots with more than 2.3 fmol of biotin-AuNP, which may be caused by the saturation of all the binding sites of the antibodies immobilized on paper through the CBM3-ZZ.

4.1.6 Rehydration of AuNPs spoted on paper

The possibility of rehydration of gold nanoparticles pre-deposited on paper spots was tested by applying either 5 pmol of antibiotin IgG in 2 µL TST, or CBM3-ZZ:antibiotin IgG conjugate (2 pmol:5 pmol) to spots with 2.3 fmol of biotin-AuNP.

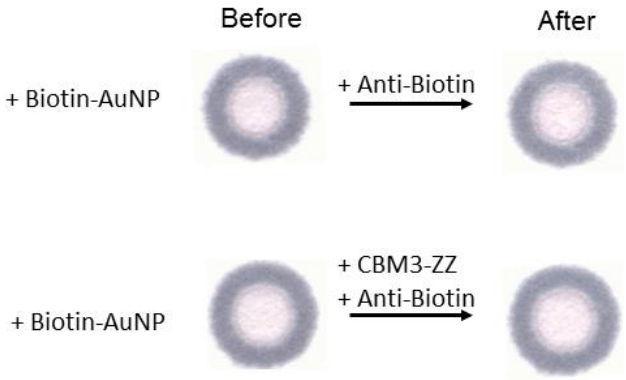

Figure 4-12 Rehydration assay of 2.31 fmol pre-deposited biotin-AuNPs by either 5 pmol of antibiotin IgG in 2 µL TST, or CBM3-ZZ:antibiotin IgG conjugate (2 pmol:5 pmol).

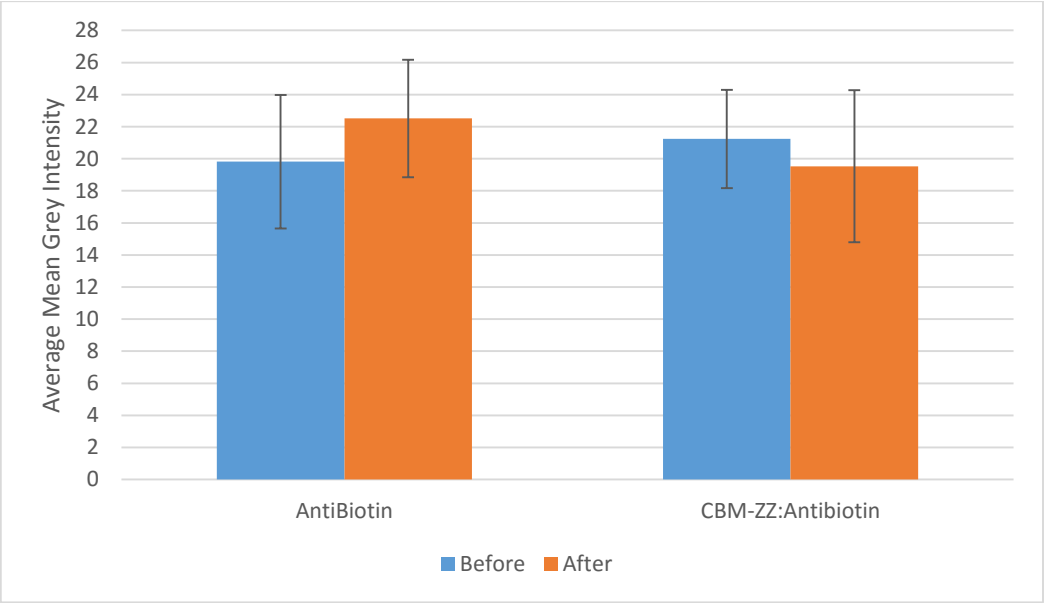

Figure 4-13 Graphic representation of the average mean grey intensity of spots before and after the rehydration of 2.3 fmol of pre-deposited biotin-AuNPs by either 5 pmol of antibiotin IgG in 2 µL TST, or CBM3-ZZ:antibiotin IgG conjugate (2 pmol:5 pmol).

Observing the spots before and after the rehydration step (Figure 4-12), there is no apparent difference in the intensity of the color by the naked eye, which is corroborated by the analysis of the spots using ImageJ. The plot of Figure 4-13 shows no significant change in the intensity of the color before and after rehydration. This means that the pre-deposited AuNPs cannot be resuspended and originate a signal similar to the one obtained when the immobilization of the antibodies is done before the application of the AuNPs.

4.2 Microfluidic Channels Assays

4.2.1 Capture of biotin-AuNPs by immobilized antibodies via CBM3-ZZ inside wax-printed channels on paper

The capture of biotin-AuNPs by antibodies immobilized in wax-printed microfluidic channels on paper via biochemical coupling with CBM3-ZZ was studied versus the physical adsorption of the antibody. To perform this assay either 5 pmol of antibiotin IgG or 2 pmol of CBM3-ZZ and 5 pmol antibiotin IgG pre-incubated were dispensed in the test zone (marked T in Figure 4-14). After drying, a sample with different quantities of biotin-AuNP was applied in the sample loading zone at the beginning of the microfluidic channel. An additional amount of buffer was added to elute the AuNPs alongside the channels.

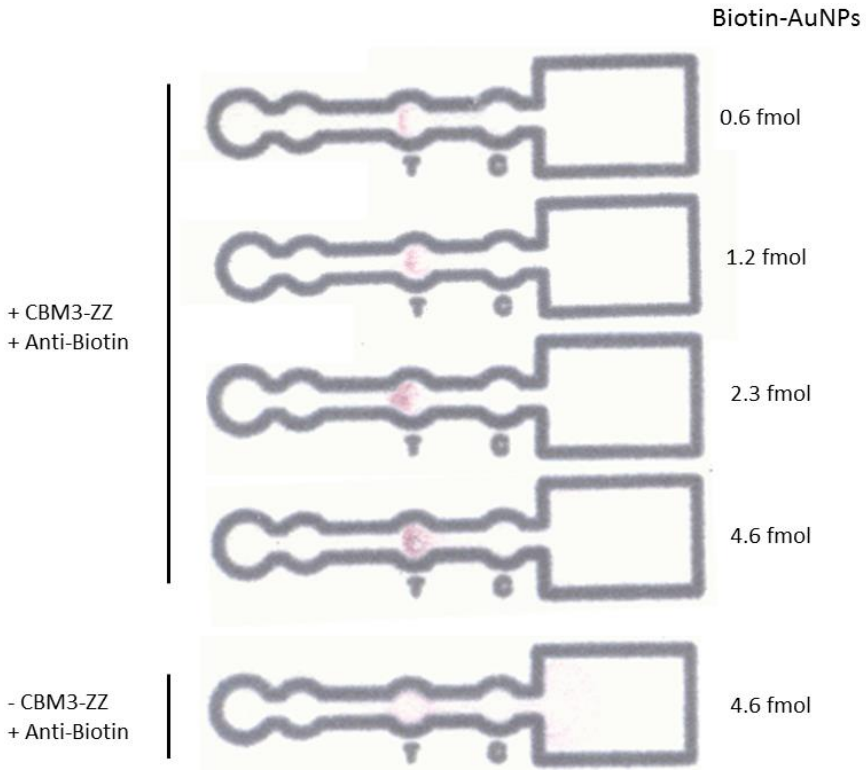

Figure 4-14 Capture of biotin-AuNPs by antibiotin IgG immobilized in paper microfluidic channels via biochemical coupling with CBM3-ZZ and physical adsorption. The bottom microfluidic channel was prepared using physical adsorption of the antibiotin IgG in the test zone, while the remaining were prepared through biochemical immobilization.

The intensity of the color developed in the test zone increases with the increasing quantities of loaded biotin-AuNPs. The µPAD prepared by physical adsorption of the antibiotin IgG does not present a signal visible with the naked eye when compared with the immobilization by biochemical coupling.

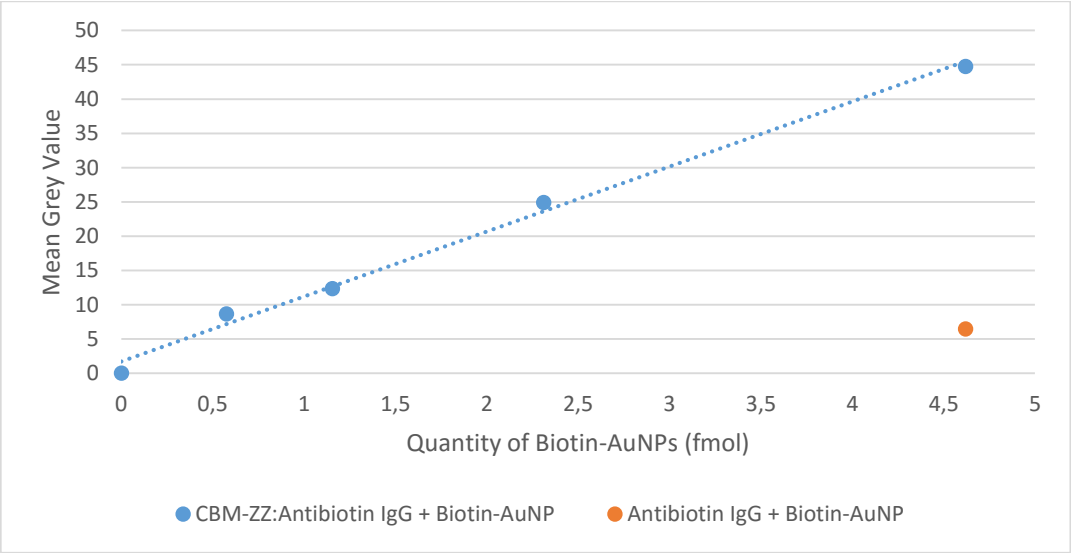

Figure 4-15 Capture of biotin-AuNPs by antibiotin IgG immobilized in paper microfluidic channels via biochemical coupling with CBM3-ZZ and physical adsorption.

The preliminary results shown in Figure 4-15, suggest a linear increase in the intensity of the color developed with increasing quantities of biotin-AuNPs in the sample added. The µPAD functionalized by physical adsorption of antibiotin IgG in the test zone shows a very low intensity of color developed, most probably because the interactions of the antibodies with the cellulose fiber are weak [8], [24]. The addition of a buffer like TST, which contains 0.05% of Tween 20, will drag the antibody through the channel. Tween 20 is a surfactant commonly used in biochemical assays to remove unbound compounds and prevent nonspecific antibody binding [8], [24]. Still some antibody molecules may be retained in the cellulose fibers that will be able to capture some of the biotin-AuNPs.

4.2.2 Conjugation studies

The ability of the different reagents to be pre-deposited on the µPAD and lead to a detectable signal in the capture zone was tested by depositing 2.3 fmol of biotin-AuNPs in spot 1, 5 pmol of either antibiotin IgG or a FITC labeled IgG antibody in spot 2 and 2 pmol of CBM-ZZ in spot 3 (Figure 4-16).

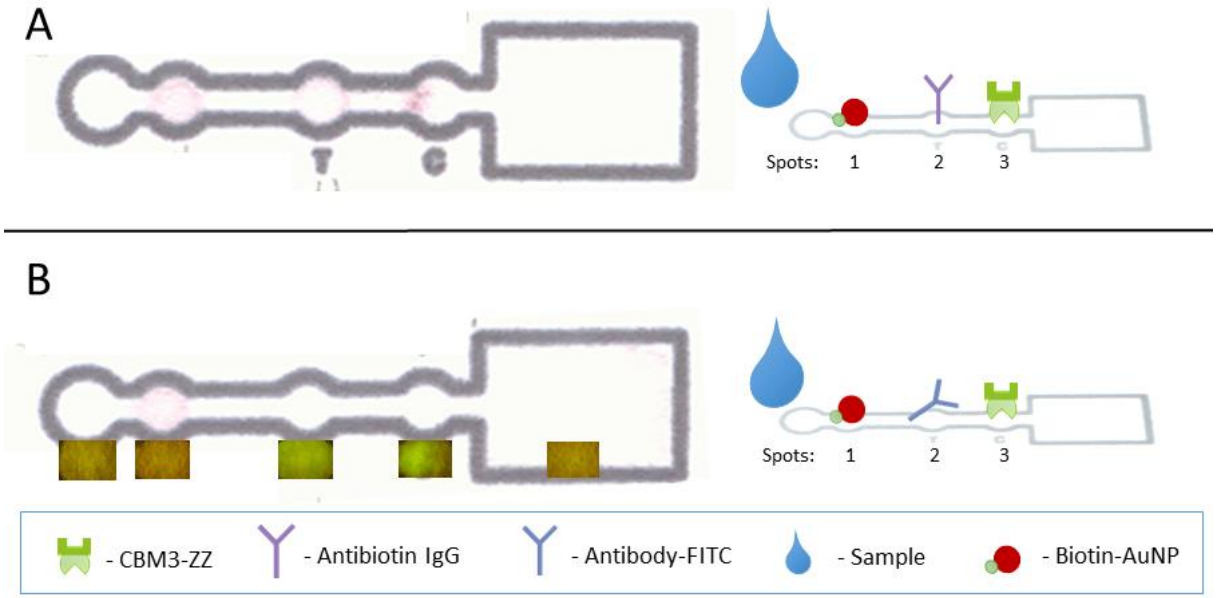

Figure 4-16 Conjugation of pre-deposited components in µPAD. At the right side of the image a schematic of the assay is drawn with the respective legend at the bottom of the image **A)** µPAD with antibiotin IgG pre-deposited in zone 2. **B)** µPAD with an IgG antibody labeled with FITC pre-deposited in zone 2.

The same procedure was done without pre-depositing the Biotin-AuNPs, and instead loading the 2.3 fmol of Biotin-AuNPs in 15 µL of TST to the sample loading zone (Figure 4-17).

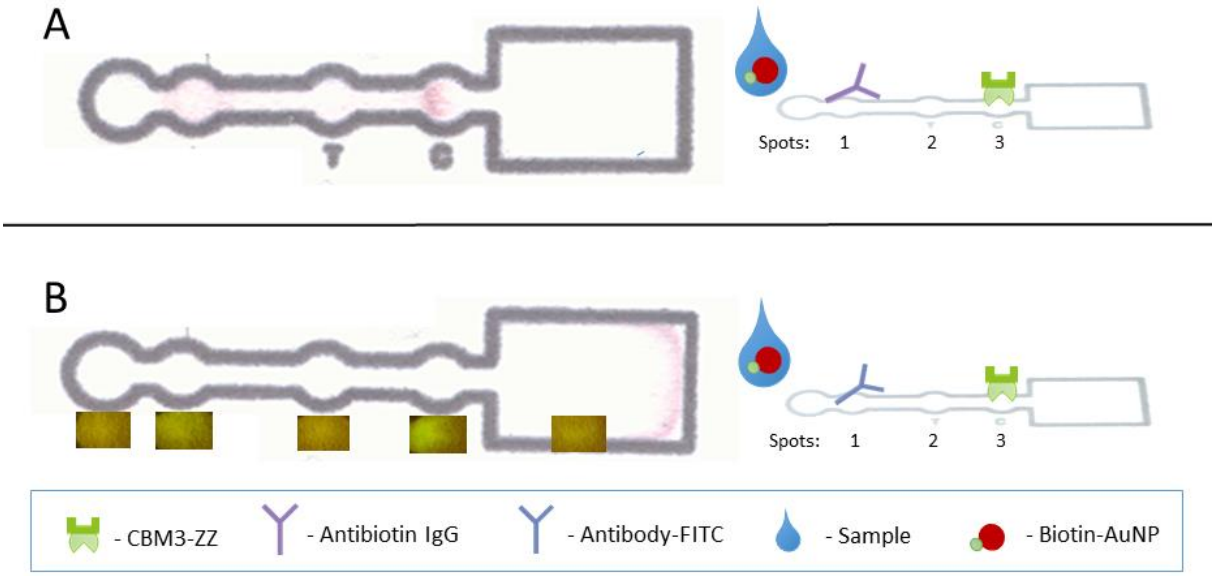

Figure 4-17 Conjugation of pre-deposited components in µPAD. At the right side of the image a schematic of the assay is drawn with the respective legend at the bottom of the image **A)** µPAD with antibiotin IgG pre-deposited in zone 1**. B)** µPAD with an IgG antibody labeled with FITC pre-deposited in zone 1.

The pre-deposition of the different components used in the immobilization and detection ability of the designed µPAD was successful (Figures 4-16 and 4-17). However, the color signal developed was not very intense, mainly due to the physical adsorption of the gold nanoparticles and the antibody which got retained in the cellulose fiber even though the microfluidic device was washed using TST which contains Tween 20, a detergent used to remove unbound compounds and prevent nonspecific antibody binding [8], [24]. Through this assay, it was possible to verify that the CBM3-ZZ has the ability to capture antibodies that are migrating alongside the channels by capillary flow. The controls performed with FITC labeled IgG antibodies (Figure 4-16B and Figure 4-17B) showed that the fluorescent antibodies were captured by the CBM3-ZZ fusion. In this case, however, and as expected, the biotin-AuNPs were not captured and accumulated in the reservoir at the end of the microfluidic devices. This means that the capture of the biotin-AuNPs is specific to the antibiotin IgG and that AuNPs are not retained by the CBM3-ZZ:antibody conjugate, i.e. there are no false positives of capture.

The ability of the conjugate CBM3-ZZ:antibitotin IgG to be formed in the µPAD during the flow of the sample by capillarity was further studied by immobilizing 2 pmol of CBM3-ZZ in both spot 2 and spot 3, and either 5 or 10 pmol of antibiotin IgG in spot 1. The µPADs were then loaded with 4.62 fmol of biotin-AuNPs in 15 µL of TST buffer in the sample loading zone (Figure 4-18).

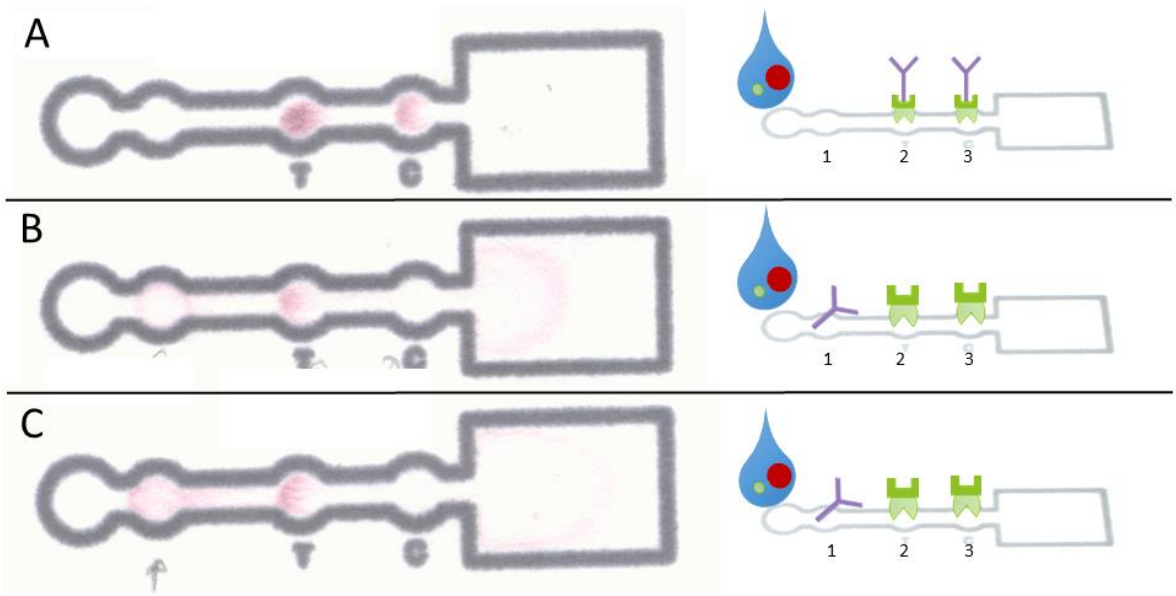

Figure 4-18 µPAD designed to study the conjugation of pre-deposited antibody. **A)** The CBM3-ZZ:antibiotin IgG conjugate was pre-incubated at room temperature and subsequently dispensed in spots 2 and 3. **B)** Immobilization of 2 pmol of CBM3-ZZ in both spot 2 and spot 3, and 5 pmol of antibiotin IgG in spot 1. **C)** Immobilization of 2 pmol of CBM3-ZZ in both spot 2 and spot 3, and 10 pmol of antibiotin IgG in spot 1.

In the µPAD of Figure 4-18A it is possible to see the saturation of the first site of capture and still a high intensity in the second spot functionalized through biochemical coupling of the CBM3-ZZ:antibiotin IgG conjugate. This test was prepared to evaluate if the weak signals obtained in both conjugation studies prior to this one were due to the pre-deposited antibodies being retained in the paper and not flowing with the presence of a buffer, or if the capture of the antibodies by the immobilized CBM-ZZ was not optimal through the migration of the antibodies by capillarity through the channel, which would lead to a capture signal in the second spot with the CBM3-ZZ immobilized.

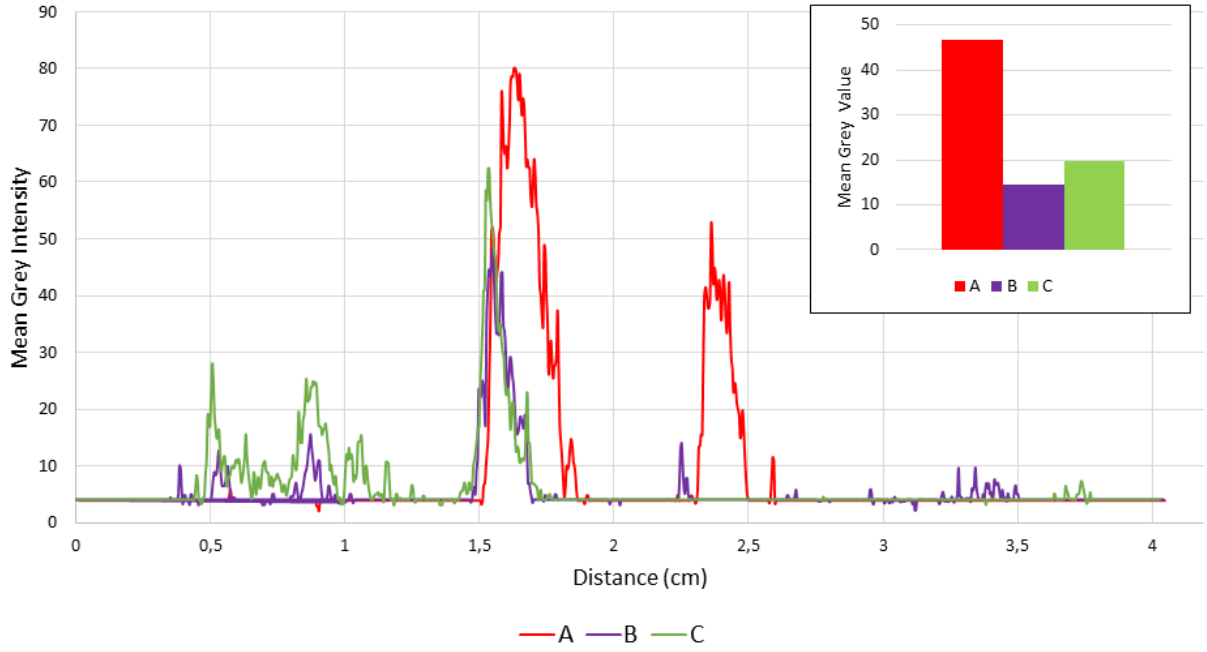

Figure 4-19 Longitudinal plot profile of the microfluidic channels shown in Figure 4-18. The letters of the legend correspond to each of the letters in Figure 4-18. In the upper right corner, a graph representing the mean grey value of the reaction zone 2 in each of the µPADs is displayed.

An observation of the µPADs B and C in Figure 4-18 and an analysis of the corresponding plot profiles in Figure 4-19 shows that the lower color intensity observed in spot 2/T is mainly due to the partial retention of the antibody (and hence of the biotin-AuNPs) in the spot where it was pre-deposited. No color is observable in spot 3/C of µPADs B and C. Since biotin-AuNPs can be seen in the reservoir on the right side of the µPADs, this indicates that the flowing antibiotin IgG was captured in spot2/T (Figure 4-18B and C). Even when the quantity of antibody pre-deposited in the µPAD was doubled, there was only a slight increase in the color intensity in the capture spot while the quantity of the physically adsorbed antibody retained in spot 1 was also higher (Figure 4-19).

4.2.3 Use of Plastic Adhesives

The effects of isolating the µPAD with an adhesive tape made of clear polyester film and acrylic medical grade adhesive was studied by using three different conditions: 1) a control without adhesive tape (Figure 3-8A); 2) a µPADs isolated underneath with the adhesive tape (Figure 3-8B); 3) a µPADs isolated underneath and above, leaving only the sample loading zone uncovered (Figure 3-8C). To each of these devices, 15 µL of an orange dye were added. A video was recorded to document the wicking of the dye (Figure 4-20).

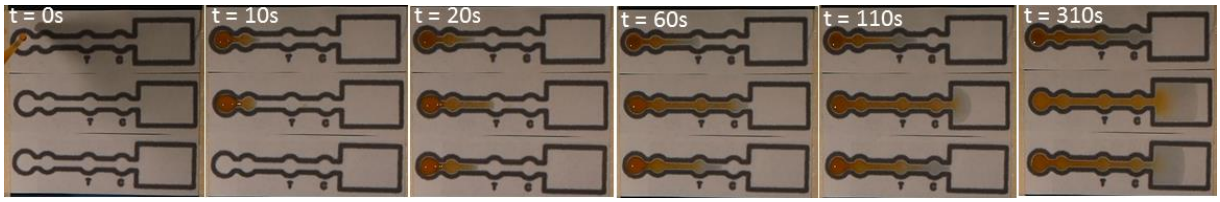

Figure 4-20 Time-lapse of the video recorded to document the capillary migration of an orange dye through the channel of the μPADs. The upper μPAD is a control without adhesive tape. The middle μPAD was isolated underneath with adhesive tape. The bottom μPAD was isolated both underneath and above, leaving only the sample loading zone uncovered. The time since the addition of the sample to the upper μPAD is indicated in the top of each frame.

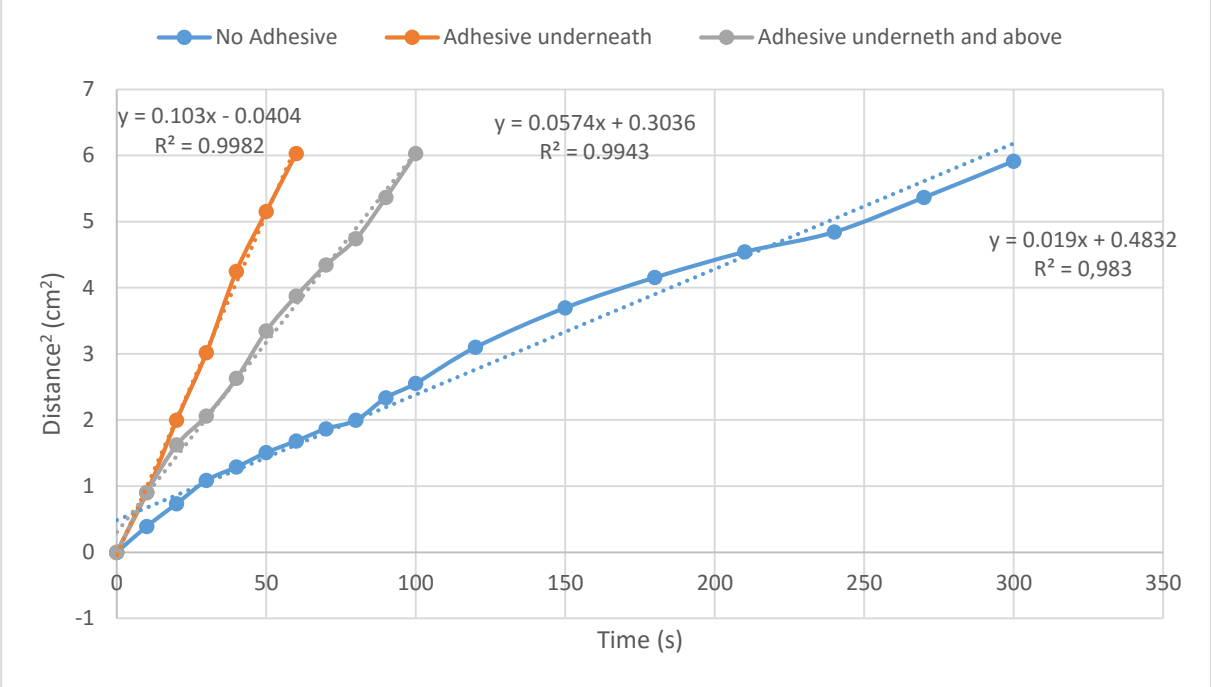

Figure 4-21 Plot of the fluid front position in each of the μPADs shown in Figure 4-20 as a function of time.

The migration of the fluid was the fastest in the μPAD with the adhesive underneath, taking 60 seconds to reach the end of the microfluidic channel (not taking into account the reservoir), followed by the μPAD with both surfaces isolated taking 100 seconds and in last place was the μPAD without adhesive tape in any of the surfaces taking 300 seconds to migrate completely through the channel.

Following this assay, a video recording of the capture of biotin-AuNPs by antibiotin IgG immobilized through biochemical coupling with CBM3-ZZ was made using the same conditions relatively to the presence/absence of adhesive tape (Figure 4-22).

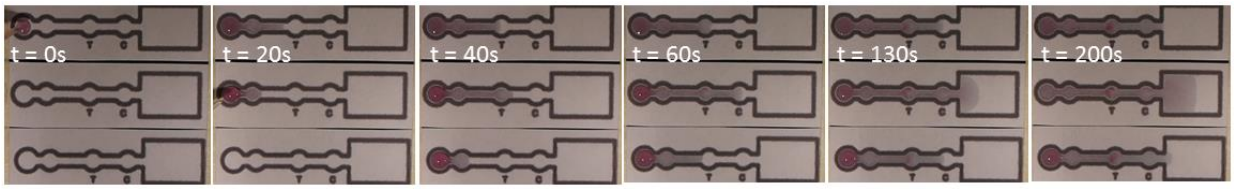

Figure 4-22 Time-lapse of the capture of biotin-AuNPs by antibiotin IgG immobilized through biochemical coupling with CBM3-ZZ. The upper μPAD is a control without adhesive tape. The middle μPAD was isolated underneath with adhesive tape. The bottom μPAD was isolated both underneath and above, leaving only the sample loading zone uncovered. The time since the addition of the sample to the upper μPAD is indicated in the top of in each frame.

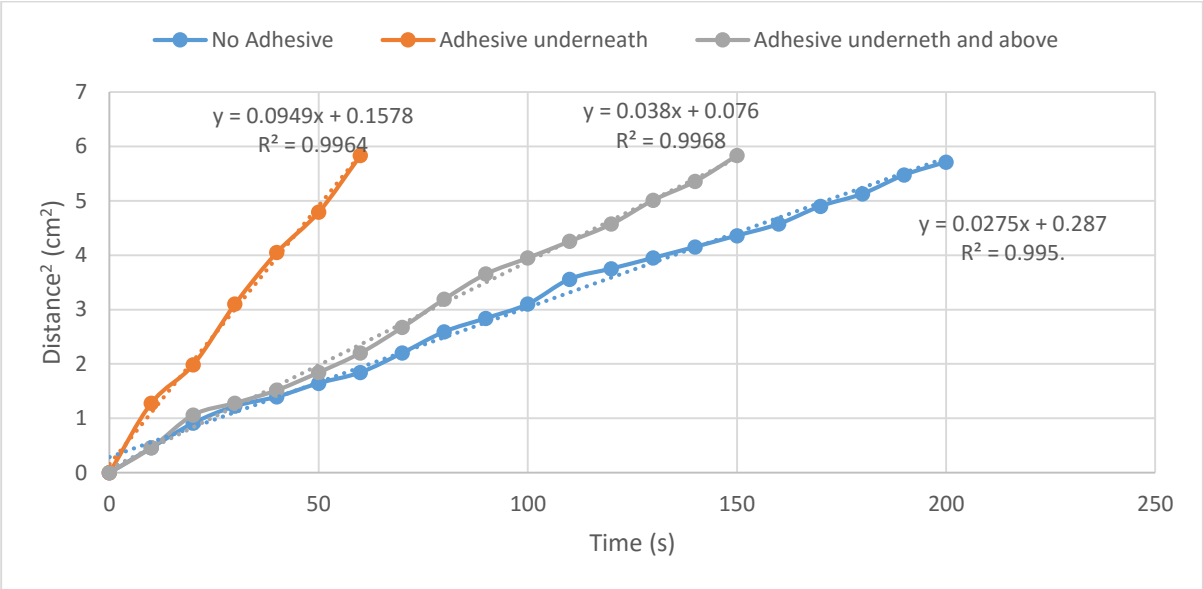

Figure 4-23 Plot of the fluid front position in each of the μPADs shown in Figure 4-22 as a function of time.

The migration of the fluid was the fastest in the μPAD with the adhesive underneath taking 60 seconds to reach the end of the microfluidic channel (not taking into account the reservoir), followed by the μPAD with both surfaces isolated taking 150 seconds and in last place was the μPAD without adhesive tape in any of the surfaces taking 200 seconds to migrate completely through the channel.

Comparing both videos, the order in which the fluid front reaches the end of the microfluidic channel, in each of the conditions, was the same, but with different timings. The data plotted in Figure 4-21 and 4-23 is done in the form of the Lucas-Washburn equation [21] (Equation 5), which describes the one-dimensional transport of a fluid in a porous matrix like a paper strip [22], [67].

$$L^2 = \frac{\gamma D}{4\eta} t \qquad (4)$$

L stands for the distance that a liquid of viscosity η and surface tension γ (which includes the effect of any contact angle dependence), penetrates into a porous material with an average pore diameter D, in time t. Thus the Washburn-like flow is characterized by $L^2 \sim t$. This implies that the fluid front velocity is decreasing with time [67]. The Washburn equation does not take into account the variation of the channel width [67], which is observable by a slight deviation in the plotted data from the trendline, which

overlaps with the fluid front reaching the different reaction zones that have a different width. Taken the Washburn equation in consideration, the variation in the velocity taken for the fluid to wick through the whole channel in the different conditions must be associated with alterations in the surface tension γ of the fluids in contact with the paper devices isolated by the adhesive tape, since there is no alteration neither to the viscosity of the liquid nor to the average pore diameter. The data suggest an increase in the surface tension when the µPAD is isolated by the adhesive tape, since the slope of the plotted data is higher (Figure 4-21 and 4-23).

The evaporation rate is higher, the larger the surface of contact with the air. This means the µPADs dry faster in the following order: i) µPAD without adhesive tape; ii) µPAD with adhesive tape underneath; iii) µPAD with adhesive tape both underneath and above. Relatively to the convenience in the handling of the µPAD, the ones isolated with adhesive tape are much more comfortable to use since there is no need to hang the µPAD in the air.

After the microfluidic devices were completely dry, the intensity of the signal concerning the capture of the biotin-AuNPs by the antibiotin IgG by CBM-ZZ immobilized in the T spot was determined using ImageJ software.

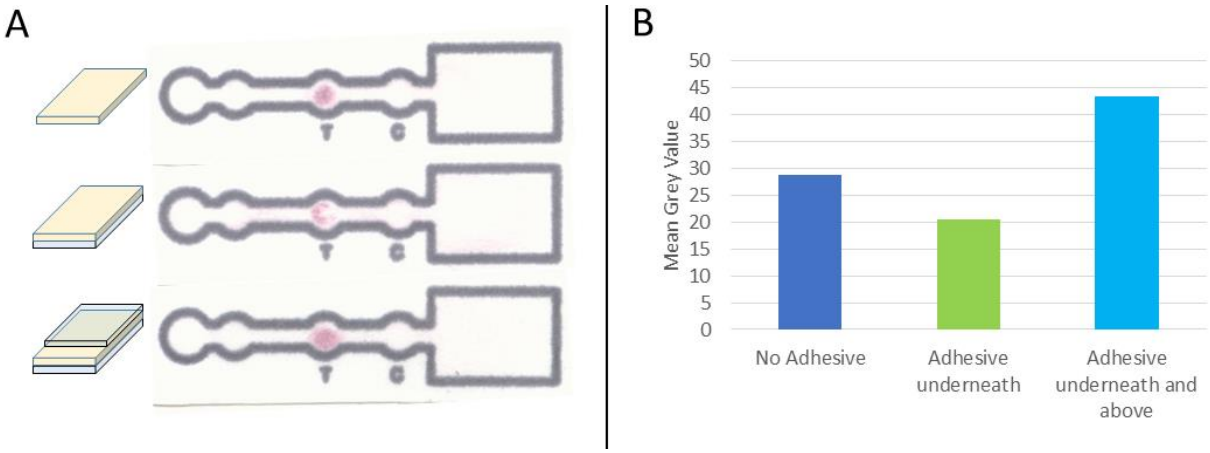

Figure 4-24 A) µPAD used in the recording of the video of the capture of biotin labeled gold nanoparticles by antibiotin IgG immobilized through biochemical coupling with CBM3-ZZ. **B)** Mean grey intensity of the spots represented in A.

The µPAD with adhesive underneath displays a weaker color than the two other conditions, this may be related with the velocity of the flow, which may have prevented the capture of the biotin-AuNPs by the antibiotin IgG. The µPAD isolated both underneath and above with the adhesive tape exhibited the highest intensity of color, this may be related to the rate of evaporation, since the µPAD stays wet during a lot more time when compared to the other, there may be a concentration effect. The acquisition of the digital images through a scanner may also be affected by the presence of the polyester film. To ascertain if the adhesive tape affected the mean grey intensity of the images acquired, in assays previously performed with the different immobilization strategies used through this thesis, images were recorded before and after the adhesive tape was applied and analyzed by ImageJ (Figure 4-25).

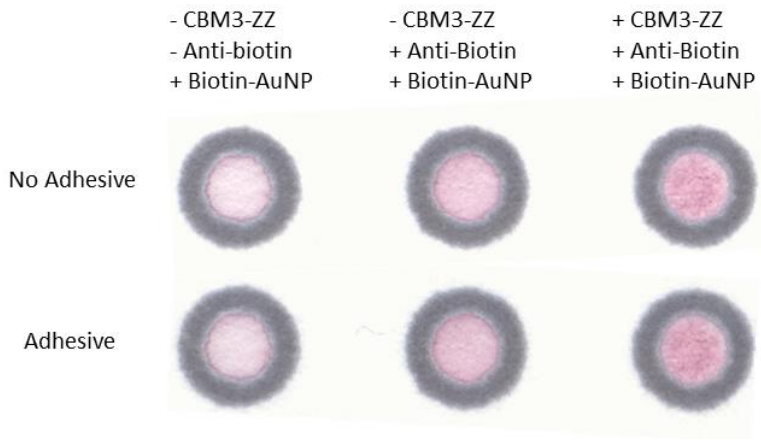

Figure 4-25 Analysis of the impact of the adhesive in the color displayed. In the top row is the digital image of the spots acquired before the adhesive tape was applied. Bottom row concerns the same spots after the adhesive tape was applied.

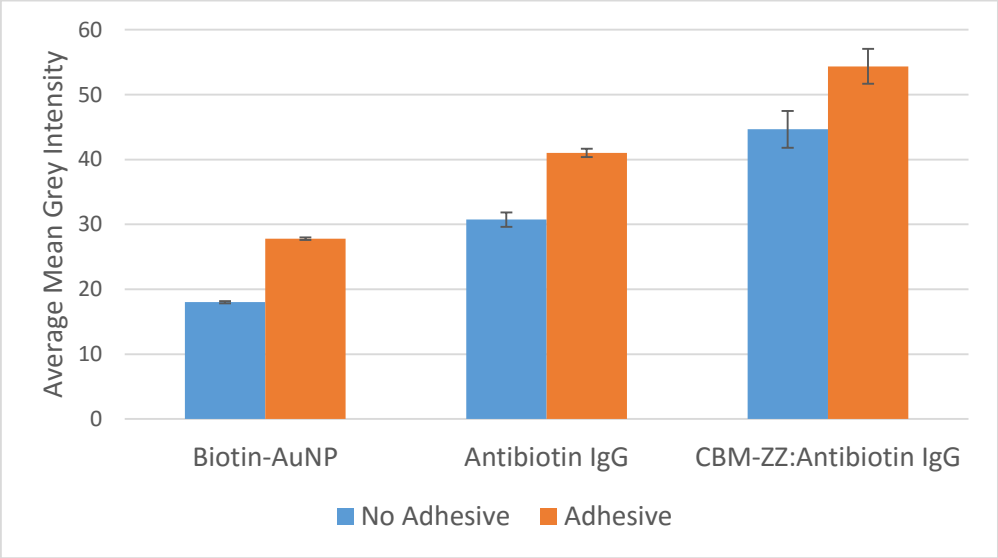

Figure 4-26 Analysis of the impact of the presence of adhesive in the color displayed. In the top row is the digital image acquired of the spots before the adhesive tape was applied. The assay was done in triplicates and the error bars represent the standard deviation.

The adhesive tape increases the mean grey intensity measured by using ImageJ as it can be seen in the data of figure 4-26, while by observation of the spots through the naked eye (Figure 4-25) no difference can be noticed. This increase in intensity may be due to a certain reflectivity of the light of the recording system when the polyester film is applied.

Chapter 5. Conclusions

Since Whitesides' group from Harvard University published the first works in μPAD, the development of this field has been growing at an accelerated pace, as it is a promising technology to develop easy-to-use and affordable disease diagnosis and environmental monitoring for both developed and developing countries. This work had as an objective, the gain of insight in the development of μPAD for immunodetection using antibodies anchored to paper through carbohydrate-binding modules fusion proteins, and gold nanoparticles as a colorimetric report agent.

The first stage of this work was to evaluate the capture ability of an antibiotin IgG immobilized on paper either by physical adsorption or biochemical coupling, in 4 mm circular reaction areas delineated by hydrophobic wax barriers. The assays using the CBM3-ZZ:antibiotin IgG complex as an immobilization approach yielded a more intense red color than the physical adsorption of the antibodies when gold nanoparticles were present. As a control, an anti-FITC IgG was used and the red color was virtually absent. SEM imaging showed that when using the antibiotin IgG immobilized by biochemical coupling the gold nanoparticles coated with biotin are uniformly distributed, while in the absence of the antibody the gold nanoparticles tend to form clusters.

The ability of the gold nanoparticles to be used as a colorimetric report agent either for a qualitative as a quantitative analysis was demonstrated, by the development of a red color of different intensity according to the quantity of gold nanoparticles applied.

The rehydration of the biotin-AuNPs pre-deposited in a spot by either the antibiotin IgG or CBM3-ZZ:antibiotin IgG was unsuccessful in the production of a signal similar to the capture assays.

The second part of the work was to evaluate the capture ability of an antibiotin IgG anchored to paper by CBM3-ZZ in a microfluidic channel with 28 mm of length (and 2.4 nominal width) plus a reservoir with 13 mm nominal length. The capture of the gold nanoparticles coated with biotin was successful, displaying an intense red color formed in the capture zone, while in a physical adsorption assay no signal is observable.

The ability to separately deposit all the components (biotin-AuNPs, antibiotin IgG, CBM3-ZZ) of the system was successful. However, the signal yielded was weaker compared to the capture assays previously described. This difference is due to part of the components being retained between the cellulose fibers and not being able to migrate through the channel, even when a surfactant is used. The improvement of the ratio of the signal yield by the components retained would be a big step to produce better μPAD so that less steps have to be done by the end user.

The isolation of the μPAD by a polyester film leads to a much more comfortable use of the microfluidic devices as the speed of the flow is higher, leading to a response slightly faster, and there is no need for a special handling by having the device hanging in the air.

The work developed in this thesis gives an insight on the development of immunoassays involving carbohydrate-binding modules as an immobilization approach and gold nanoparticles as a colorimetric report agent in microfluidic devices. One interesting continuation of this work would be the development of a μPAD based on sandwich ELISA. Using a detection system by immobilizing in paper a CBM3-ZZ:antibody IgG complex to detect a specific antigen and then use a second antibody labeled with a gold nanoparticle as the reporting agent.

Chapter 6. References

[1] D. M. Cate, J. A. Adkins, J. Mettakoonpitak, and C. S. Henry, “Recent developments in paper-based microfluidic devices,” *Anal. Chem.*, vol. 87, no. 1, pp. 19–41, 2015.

[2] X. Li, D. R. Ballerini, and W. Shen, “A perspective on paper-based microfluidics: Current status and future trends,” *Biomicrofluidics*, vol. 6, no. 2012, 2012.

[3] V. Leung, “Development of paper-based devices for diagnostics and biosensing,” *Access*, pp. viii, 44, 2011.

[4] F. Kong and Y. F. Hu, “Biomolecule immobilization techniques for bioactive paper fabrication,” *Anal. Bioanal. Chem.*, vol. 403, pp. 7–13, 2012.

[5] E. W. Nery and L. T. Kubota, “Sensing approaches on paper-based devices: A review,” *Anal. Bioanal. Chem.*, vol. 405, pp. 7573–7595, 2013.

[6] M. M. Mentele, J. Cunningham, K. Koehler, J. Volckens, and C. S. Henry, “Microfluidic paper-based analytical device for particulate metals,” *Anal. Chem.*, vol. 84, no. 10, pp. 4474–4480, 2012.

[7] G. a. Posthuma-Trumpie, J. Korf, and A. Van Amerongen, “Lateral flow (immuno)assay: Its strengths, weaknesses, opportunities and threats. A literature survey,” *Anal. Bioanal. Chem.*, vol. 393, pp. 569–582, 2009.

[8] R. Pelton, “Bioactive paper provides a low-cost platform for diagnostics,” *TrAC - Trends Anal. Chem.*, vol. 28, no. 8, pp. 925–942, 2009.

[9] E. Carrilho, A. W. Martinez, and G. M. Whitesides, “Understanding wax printing a simple micropatterning process for paper based microfluidics,” vol. 81, no. 16, pp. 7091–7095, 2009.

[10] A. W. Martinez, S. T. Phillips, G. M. Whitesides, and E. Carrilho, “Diagnostics for the developing world: Microfluidic paper-based analytical devices,” *Anal. Chem.*, vol. 82, no. 1, pp. 3–10, 2010.

[11] A. W. Martinez, S. T. Phillips, M. J. Butte, and G. M. Whitesides, “Patterned paper as a platform for inexpensive, low-volume, portable bioassays,” *Angew. Chemie - Int. Ed.*, vol. 46, no. 8, pp. 1318–1320, 2007.

[12] D. A. Bruzewicz, M. Reches, and G. M. Whitesides, “Low-cost printing of poly(dimethylsiloxane) barriers to define microchannels in paper,” *Anal. Chem.*, vol. 80, pp. 3387–3392, 2008.

[13] K. Abe, K. Suzuki, and D. Citterio, “Inkjet-printed microfluidic multianalyte chemical sensing paper,” *Anal. Chem.*, vol. 80, pp. 6928–6934, 2008.

[14] X. Li, J. Tian, T. Nguyen, and W. Shen, “Paper-based microfluidic devices by plasma treatment,” *Anal. Chem.*, vol. 80, pp. 9131–9134, 2008.

[15] E. M. Fenton, M. R. Mascarenas, G. P. López, and S. S. Sibbett, “Multiplex lateral-flow test strips

fabricated by two-dimensional shaping," *ACS Appl. Mater. Interfaces*, vol. 1, pp. 124–129, 2009.

[16] M. S. Khan, D. Fon, X. Li, J. Tian, J. Forsythe, G. Garnier, and W. Shen, "Biosurface engineering through ink jet printing," *Colloids Surfaces B Biointerfaces*, vol. 75, pp. 441–447, 2010.

[17] J. Olkkonen, K. Lehtinen, and T. Erho, "Flexographically printed fluidic structures in paper," *Anal. Chem.*, vol. 82, no. 24, pp. 10246–10250, 2010.

[18] Z. Nie, C. A. Nijhuis, J. Gong, X. Chen, A. Kumachev, A. W. Martinez, M. Narovlyansky, and G. M. Whitesides, "Electrochemical sensing in paper-based microfluidic devices.," *Lab Chip*, vol. 10, pp. 477–483, 2010.

[19] G. Chitnis, Z. Ding, C.-L. Chang, C. A. Savran, and B. Ziaie, "Laser-treated hydrophobic paper: an inexpensive microfluidic platform.," *Lab Chip*, vol. 11, pp. 1161–1165, 2011.

[20] R. Lu, W. Shi, L. Jiang, J. Qin, and B. Lin, "Rapid prototyping of paper-based microfluidics with wax for low-cost, portable bioassay," *Electrophoresis*, vol. 30, no. 9, pp. 1497–1500, 2009.

[21] E. W. Washburn, "The dynamics of capillary flow," *Phys. Rev.*, vol. 17, no. 3, pp. 273–283, 1921.

[22] B. R. Lutz, P. Trinh, C. Ball, E. Fu, and P. Yager, "Two-dimensional paper networks: programmable fluidic disconnects for multi-step processes in shaped paper," *Lab Chip*, vol. 11, p. 4274, 2011.

[23] T. Vo-Dinh and B. Cullum, "Biosensors and biochips: advances in biological and medical diagnostics.," *Fresenius. J. Anal. Chem.*, vol. 366, no. 2000, pp. 540–551, 2008.

[24] A. M. M. Rosa, a F. Louro, S. a M. Martins, J. Inácio, A. M. Azevedo, and D. M. F. Prazeres, "Capture and detection of DNA hybrids on paper via the anchoring of antibodies with fusions of carbohydrate binding modules and ZZ-domains.," *Anal. Chem.*, vol. 86, pp. 4340–7, 2014.

[25] O. Shoseyov, Z. Shani, and I. Levy, "Carbohydrate binding modules: biochemical properties and novel applications.," *Microbiol. Mol. Biol. Rev.*, vol. 70, no. 2, pp. 283–295, 2006.

[26] A. W. Martinez, S. T. Phillips, Z. Nie, C.-M. Cheng, E. Carrilho, B. J. Wiley, and G. M. Whitesides, "Programmable diagnostic devices made from paper and tape.," *Lab Chip*, vol. 10, pp. 2499–2504, 2010.

[27] A. K. Yetisen, M. S. Akram, and C. R. Lowe, "Paper-based microfluidic point-of-care diagnostic devices.," *Lab Chip*, vol. 13, no. 12, pp. 2210–51, 2013.

[28] B. J. Toley, B. McKenzie, T. Liang, J. R. Buser, P. Yager, and E. Fu, "Tunable-Delay Shunts for Paper Micro fl uidic Devices," *Anal. Chem.*, vol. 85, pp. 11545–52, 2013.

[29] J. Houghtaling, T. Liang, G. Thiessen, and E. Fu, "Dissolvable bridges for manipulating fluid volumes in paper networks," *Anal. Chem.*, vol. 85, pp. 11201–11204, 2013.

[30] M. M. Gong, P. Zhang, B. D. MacDonald, and D. Sinton, "Nanoporous membranes enable

concentration and transport in fully wet paper-based assays.," *Anal. Chem.*, vol. 86, no. 16, pp. 8090–7, 2014.

[31] A. W. Martinez, S. T. Phillips, E. Carrilho, S. W. Thomas, H. Sindi, and G. M. Whitesides, "Simple telemedicine for developing regions: Camera phones and paper-based microfluidic devices for real-time, off-site diagnosis," *Anal. Chem.*, vol. 80, no. 10, pp. 3699–3707, 2008.

[32] M. Faraday, "AuNP117-The Bakerian Lecture: Experimental Relations of Gold (and Other Metals) to Light," *Philos. Trans. R. Soc. London*, vol. 147, no. 0, pp. 145–181, 1857.

[33] X. Liu, M. Atwater, J. Wang, and Q. Huo, "Extinction coefficient of gold nanoparticles with different sizes and different capping ligands.," *Colloids Surf. B. Biointerfaces*, vol. 58, no. 1, pp. 3–7, 2007.

[34] M. C. Daniel and D. Astruc, "Gold Nanoparticles: Assembly, Supramolecular Chemistry, Quantum-Size-Related Properties, and Applications Toward Biology, Catalysis, and Nanotechnology," *Chem. Rev.*, vol. 104, no. 1, pp. 293–346, 2004.

[35] T. a Taton, C. a Mirkin, and R. L. Letsinger, "Scanometric DNA array detection with nanoparticle probes.," *Science*, vol. 289, no. 5485, pp. 1757–1760, 2000.

[36] W. Zhao, M. M. Ali, S. D. Aguirre, M. a. Brook, and Y. Li, "Paper-based bioassays using gold nanoparticle colorimetric probes," *Anal. Chem.*, vol. 80, no. 22, pp. 8431–8437, 2008.

[37] J. Turkevich, P. C. Stevenson, and J. Hillier, "A study of the nucleation and growth processes in the synthesis of colloidal gold," *Discuss. Faraday Soc.*, vol. 11, no. 0, pp. 55–75, 1951.

[38] G. Frens, "Controlled Nucleation for the Regulation of the Particle Size in Monodisperse Gold Suspensions," *Nat. Phys. Sci.*, vol. 241, no. 105, pp. 20–22, 1973.

[39] D. Quesada-González and A. Merkoçi, "Nanoparticle-based lateral flow biosensors," *Biosens. Bioelectron.*, vol. 73, pp. 47–63, 2015.

[40] D. D. Liana, B. Raguse, J. Justin Gooding, and E. Chow, "Recent advances in paper-based sensors," *Sensors (Switzerland)*, vol. 12, no. 9, pp. 11505–11526, 2012.

[41] L. Ge, S. Wang, X. Song, S. Ge, and J. Yu, "3D Origami-based multifunction-integrated immunodevice: low-cost and multiplexed sandwich chemiluminescence immunoassay on microfluidic paper-based analytical device," *Lab on a Chip*, vol. 12. p. 3150, 2012.

[42] M. S. Khan, G. Thouas, W. Shen, G. Whyte, and G. Garnier, "Paper diagnostic for instantaneous blood typing," *Anal. Chem.*, vol. 82, pp. 4158–4164, 2010.

[43] A. Apilux, W. Dungchai, W. Siangproh, N. Praphairaksit, C. S. Henry, and O. Chailapakul, "Lab-on-paper with dual electrochemical/colorimetric detection for simultaneous determination of gold and iron.," *Anal. Chem.*, vol. 82, pp. 1727–1732, 2010.

[44] S. M. Z. Hossain, R. E. Luckham, M. J. McFadden, and J. D. Brennan, "Reagentless bidirectional

lateral flow bioactive paper sensors for detection of pesticides in beverage and food samples," *Anal. Chem.*, vol. 81, pp. 9055–9064, 2009.

[45] E. a. Bayer, R. Lamed, B. a. White, and H. J. Flints, "From cellulosomes to cellulosomics," *Chem. Rec.*, vol. 8, no. 6, pp. 364–377, 2008.

[46] A. B. Boraston, D. N. Bolam, H. J. Gilbert, and G. J. Davies, "Carbohydrate-binding modules: fine-tuning polysaccharide recognition.," *Biochem. J.*, vol. 382, pp. 769–781, 2004.

[47] J. E. Hyeon, S. D. Jeon, and S. O. Han, "Cellulosome-based, Clostridium-derived multi-functional enzyme complexes for advanced biotechnology tool development: Advances and applications," *Biotechnol. Adv.*, vol. 31, no. 6, pp. 936–944, 2013.

[48] N. R. Gilkes, R. a. Warren, R. C. Miller, and D. G. Kilburn, "Precise excision of the cellulose binding domains from two Cellulomonas fimi cellulases by a homologous protease and the effect on catalysis.," *J. Biol. Chem.*, vol. 263, no. 21, pp. 10401–10407, 1988.

[49] "CAZY: Carbohydrate-binding module family classification." [Online] [Cited: 21 of October of 2015] http://www.cazy.org/Carbohydrate-Binding-Modules.html".

[50] A. B. Boraston, E. Ficko-Blean, and M. Healey, "Carbohydrate recognition by a large sialidase toxin from Clostridium perfringens," *Biochemistry*, vol. 46, no. 40, pp. 11352–11360, 2007.

[51] C. M. G. a Fontes and H. J. Gilbert, "Cellulosomes: highly efficient nanomachines designed to deconstruct plant cell wall complex carbohydrates.," *Annu. Rev. Biochem.*, vol. 79, pp. 655–681, 2010.

[52] W. Lewis, E. Keshavarz-Moore, J. Windust, D. Bushell, and N. Parry, "Construction and evaluation of novel fusion proteins for targeted delivery of micro particles to cellulose surfaces.," *Biotechnol. Bioeng.*, vol. 94, no. 4, pp. 625–632, 2006.

[53] G. Hussack, Y. Luo, L. Veldhuis, J. C. Hall, J. Tanha, and R. MacKenzie, "Multivalent anchoring and oriented display of single-domain antibodies on cellulose," *Sensors*, vol. 9, pp. 5351–5367, 2009.

[54] M. Tolba, O. Minikh, L. Y. Brovko, S. Evoy, and M. W. Griffiths, "Oriented immobilization of bacteriophages for biosensor applications.," *Appl. Environ. Microbiol.*, vol. 76, no. 2, pp. 528–35, 2010.

[55] I. Lee, B. R. Evans, and J. Woodward, "The mechanism of cellulase action on cotton fibers: Evidence from atomic force microscopy," *Ultramicroscopy*, vol. 82, no. 1–4, pp. 213–221, 2000.

[56] J. A. Francisco, C. Stathopoulos, R. A. Warren, D. G. Kilburn, and G. Georgiou, "Specific adhesion and hydrolysis of cellulose by intact Escherichia coli expressing surface anchored cellulase or cellulose binding domains," *Bio/Technology*, vol. 11, no. 4, pp. 491–495, 1993.

[57] E. Ong, "The cellulose-binding domains of cellulases: tools for biotechnology," *Trends*

Biotechnol., vol. 7, no. 9, pp. 239–243, 1989.

[58] O. Yaniv, G. Fichman, I. Borovok, Y. Shoham, E. a. Bayer, R. Lamed, L. J. W. Shimon, and F. Frolow, “Fine-structural variance of family 3 carbohydrate-binding modules as extracellular biomass-sensing components of Clostridium thermocellum anti-σI factors,” *Acta Crystallogr. Sect. D Biol. Crystallogr.*, vol. 70, no. 2, pp. 522–534, 2014.

[59] O. Yaniv, E. Morag, I. Borovok, E. a. Bayer, R. Lamed, F. Frolow, and L. J. W. Shimon, “Structure of a family 3a carbohydrate-binding module from the cellulosomal scaffoldin CipA of Clostridium thermocellum with flanking linkers: Implications for cellulosome structure,” *Acta Crystallogr. Sect. F Struct. Biol. Cryst. Commun.*, vol. 69, no. 7, pp. 733–737, 2013.

[60] G. Carrard, a Koivula, H. Söderlund, and P. Béguin, “Cellulose-binding domains promote hydrolysis of different sites on crystalline cellulose.,” *Proc. Natl. Acad. Sci. U. S. A.*, vol. 97, no. 19, pp. 10342–10347, 2000.

[61] J. Tormo, R. Lamed, A. . J. Chirino, E. Morag, E. . a Bayer, Y. Shoham, and T. A. a Steitz, “Crystal structure of a bacterial family-III cellulose-binding domain: a general mechanism for attachment to cellulose.,” *EMBO J.*, vol. 15, no. 21, pp. 5739–5751, 1996.

[62] J. C. Jokerst, J. a. Adkins, B. Bisha, M. M. Mentele, L. D. Goodridge, and C. S. Henry, “Development of a paper-based analytical device for colorimetric detection of select foodborne pathogens,” *Anal. Chem.*, vol. 84, pp. 2900–2907, 2012.

[63] P. J. Yunker, T. Still, M. a Lohr, and a G. Yodh, “Suppression of the coffee-ring effect by shape-dependent capillary interactions.,” *Nature*, vol. 476, no. 7360, pp. 308–11, 2011.

[64] “Cytodiagnostics: Gold nanoparticles properties. [Online] [14 of November of 2015] http://www.cytodiagnostics.com/store/pc/Gold-Nanoparticle-Properties-d2.html.”

[65] “NanoComposix - Gold Nanoparticles:Optical Properties. [Online] [14 of November of 2015]http://nanocomposix.eu/pages/gold-nanoparticles-optical-properties#aggregation.”.

[66] “Back-scattered Electron Detector (BSE). [Online] [14 of November of 2015] http://serc.carleton.edu/researcheducation/geochemsheets/bse.html.”.

[67] E. Fu, S. A. Ramsey, P. Kauffman, B. Lutz, and P. Yager, “Transport in two-dimensional paper networks.,” *Microfluid. Nanofluidics*, vol. 10, no. 1, pp. 29–35, 2011.